

Multi-view Graph Learning by Joint Modeling of Consistency and Inconsistency

Youwei Liang, Dong Huang, *Member, IEEE*, Chang-Dong Wang, *Member, IEEE*,
and Philip S. Yu, *Fellow, IEEE*

Abstract—Graph learning has emerged as a promising technique for multi-view clustering with its ability to learn a unified and robust graph from multiple views. However, existing graph learning methods mostly focus on the multi-view consistency issue, yet often neglect the inconsistency across multiple views, which makes them vulnerable to possibly low-quality or noisy datasets. To overcome this limitation, we propose a new multi-view graph learning framework, which for the first time simultaneously and explicitly models multi-view *consistency* and multi-view *inconsistency* in a unified objective function, through which the consistent and inconsistent parts of each single-view graph as well as the unified graph that fuses the consistent parts can be iteratively learned. Though optimizing the objective function is NP-hard, we design a highly efficient optimization algorithm which is able to obtain an approximate solution with linear time complexity in the number of edges in the unified graph. Furthermore, our multi-view graph learning approach can be applied to both similarity graphs and dissimilarity graphs, which lead to two graph fusion-based variants in our framework. Experiments on twelve multi-view datasets have demonstrated the robustness and efficiency of the proposed approach.

Index Terms—Clustering; Multi-view graph learning; Multi-view clustering; Graph fusion; Consistency; Inconsistency.

1 INTRODUCTION

MULTI-VIEW data consist of features collected from multiple heterogeneous sources (or views). Multiple views of features can provide rich and complementary information for discovering the underlying cluster structure of data. It has been a popular research topic in recent years as to how to exploit the features effectively and jointly from multiple views and thus achieve robust clustering results for multi-view data.

In the literature, numerous (single-view) clustering methods have been developed [1], among which the graph-based methods are one of the most widely-studied categories [2], [3], [4]. The graph-based methods typically construct a graph structure, and then partition the graph to obtain the clustering result. In these methods, the construction of the graph is independent of clustering, and the clustering performance heavily relies on the predefined graph. To alleviate this limitation, some graph learning methods have been presented [5], [6], where the graph structure can be adaptively learned in the clustering process. Recently, inspired by the single-view graph learning [5], [6], the multi-view graph learning has rapidly emerged as a powerful technique for enhancing the multi-view clustering performance [7], [8], [9], [10]. Notably, Zhan et al. [7], [8], [9] developed several multi-view graph learning approaches which

are able to fuse multiple graphs into a unified graph with desired number of connected components. Nie et al. [10] proposed a self-weighted scheme for fusing multiple graphs with the importance of each view considered. Despite the significant progress, a common limitation to these multi-view graph learning methods lies in that they mostly focus on the consistency of multiple views, but lack the ability to explicitly consider both multi-view consistency and inconsistency (which may be brought in by noise, corruptions, or view-specific characteristics) in their frameworks, which may degrade their performances when faced with complex or possibly noisy data.

To deal with the potential noise or corruptions in a graph, Bojchevski et al. [11] proposed a new graph-based clustering method based on the latent decomposition of the similarity graph into two graphs, namely, the *good* graph and the *corrupted* graph. Though it is able to learn a good graph by eliminating the influence of potential noise, this graph learning method [11] is only applicable to a single graph (for a single view) and cannot be utilized in the multi-view graph learning task where multiple graphs from multiple views are involved. Thereby, how to jointly model the multi-view consistency (which can be viewed as the multi-view good graphs) and the multi-view inconsistency (which can be viewed as the multi-view corrupted graphs) in a unified graph learning model to improve multi-view clustering performance is still an open problem.

To tackle this problem, this paper proposes a novel multi-view graph learning approach, which is further applied to multi-view clustering. In this paper, we argue that the simultaneous modeling of multi-view consistency and inconsistency can significantly benefit the multi-view graph learning process. In particular, with the graph structures of multiple views given, their consistency and inconsistency are simultaneously leveraged to learn a unified graph. It

- Y. Liang and D. Huang are with the College of Mathematics and Informatics, South China Agricultural University, Guangzhou, China. E-mail: liangyouwei1@gmail.com, huangdonghere@gmail.com.
- C.-D. Wang is with the School of Data and Computer Science, Sun Yat-sen University, Guangzhou, China, and also with Guangdong Key Laboratory of Information Security Technology, Guangzhou, China, and also with Key Laboratory of Machine Intelligence and Advanced Computing, Ministry of Education, China. E-mail: changdongwang@hotmail.com.
- P. S. Yu is with Department of Computer Science, University of Illinois at Chicago, Chicago, IL 60607, USA. E-mail: psyu@cs.uic.edu

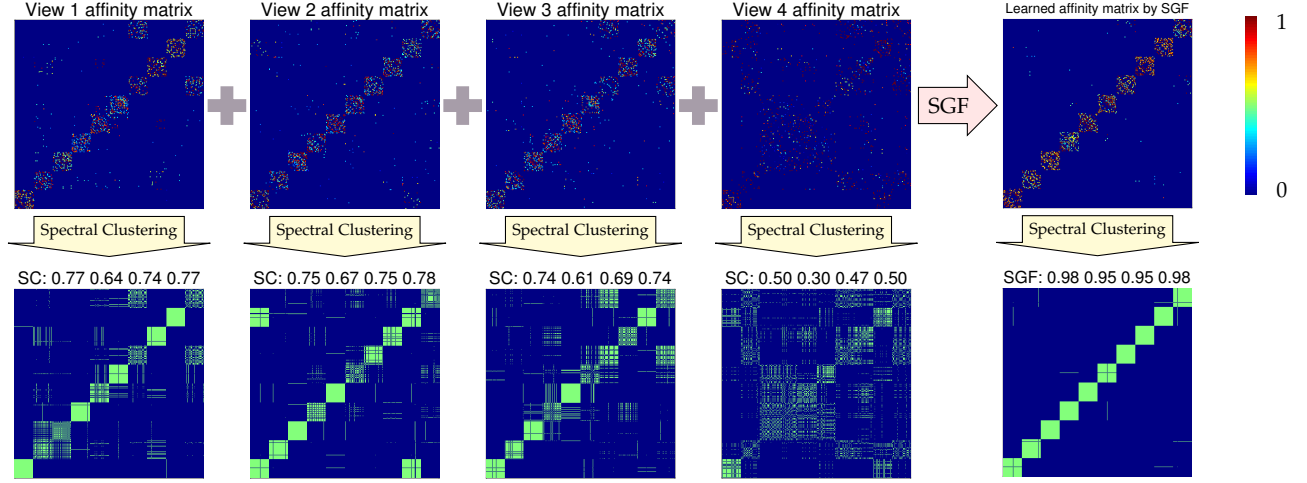


Fig. 1. Visualization of the affinity (similarity) matrices of the UCI Handwritten Digit dataset. Four views are used to learn the unified graph and the number of k NN is 15. The first row corresponds to the four single-view affinity matrices and the learned affinity matrix (i.e., the unified graph) by our multi-view graph learning framework SGF. The second row corresponds to the clustering results by performing spectral clustering (SC) on the single-view graph and the learned graph. The four numbers on each figure are the clustering scores ACC, ARI, NMI and purity, respectively.

is intuitive to assume that the graph of each view can be decomposed into two parts, i.e., the consistent part and the inconsistent part, and the goal is to learn and remove the inconsistent (or noisy) parts while preserving the consistent parts. Specifically, we formulate the multi-view consistency and multi-view inconsistency as well as the graph fusion term into a new objective function. By iteratively optimizing the objective function, the multi-view graph decomposition and the multi-view graph fusion are simultaneously achieved. With the fused graph obtained, some conventional graph-based methods like spectral clustering can be performed to obtain the final multi-view clustering result. For clarity, we provide a visual example for our multi-view graph learning model in Figure 1. As shown in the first row of Figure 1, the four similarity (affinity) matrices from four views appear to be corrupted to different extents, and our similarity graph fusion (SGF) method can effectively remove most of these corruptions (or inconsistency) while yielding a unified and better graph with their consistent parts fused and strengthened. As shown in the second row in Figure 1, by graph fusion with both consistency and inconsistency considered, the final clustering (in the fifth column) on the fused graph is significantly better than the clustering on the single-view graphs. It also shows that the proposed approach is able to achieve superior performance at the presence of some highly corrupted graph (e.g., the fourth single-view graph).

For clarity, the main contributions of this work are summarized as follows.

- We propose a novel multi-view graph learning approach, which for the first time, to the best of our knowledge, simultaneously and explicitly models multi-view consistency and multi-view inconsistency in a unified objective function, where multi-view consistency can be iteratively learned and fused into a unified graph as the multi-view inconsistency is

automatically identified and removed.

- Although optimizing the objective function is NP-hard, we design a highly efficient algorithm to obtain an approximate solution by theoretically analyzing the properties of the objective function and constraints, which has basically linear time complexity in the number of edges in the graphs or in the number of nodes in the k NN graphs.
- A novel multi-view clustering framework based on multi-view graph learning is presented, which is further extended into two graph fusion variants, corresponding to distance (dissimilarity) graph fusion (DGF) and similarity graph fusion (SGF), respectively. DGF and SGF have shown superior performance over the state-of-the-art multi-view clustering algorithms in extensive experiments.
- The proposed algorithms perform stably across a wide range of parameters. Even without dataset-specific parameter tuning, our algorithms can still achieve stably high-quality clustering results on various multi-view datasets.

A preliminary version of this paper was reported in [12]. In this paper, we have made significant revisions and added substantial analysis for the proposed framework. Firstly, we have almost completely revised the optimization algorithm, which improves the efficiency and stability of the proposed framework. In particular, we have gained deeper understandings of the properties of the optimization problem (e.g., Lemma 1, Lemma 2, and Section 4.2, 4.3, 4.4.1, 4.6), which leads to solving the optimization problem more efficiently and stably than the projection method in [12]. Moreover, our theoretical analysis shows that the objective function can be rewritten as the sum of many quadratic functions that share a Hessian matrix, which allows us to modify the d.c. algorithm [13] to optimize these quadratic functions all at once. Secondly, as a consequence of im-

proved stability, the proposed framework with the new optimization method can learn a good graph even without dataset-specific parameter tuning, which will be reported in the Appendix. Thirdly, we theoretically show that the time complexity of the new optimization approach is basically linear in the number of edges in the multi-view graphs or in the number of nodes in the k NN graphs, even though exactly solving the problem is NP-hard. Fourthly, we introduce multi-view dense representation to replace the sparse matrix used in [12] that consumes three times larger memory and is less efficient. And a graph normalization method is added to the two graph fusion algorithms (SGF and DGF), which improves the performance of clustering. Fifthly, we introduce view-specific weights for every view in our framework so that users can force the unified graph closer to the important views. Last but not least, the experimental section is substantially extended, where more benchmark datasets are used and more experimental comparison and analysis are provided, which further demonstrate the effectiveness and robustness of the proposed framework. The code for this paper is available at GitHub¹.

The rest of this paper is organized as follows. In Section 2, we review the related work in multi-view clustering, especially in multi-view graph learning. In Section 3, we propose the novel multi-view graph learning framework. In Section 4, we theoretically analyze the optimization problem in our framework and present a highly efficient algorithm to solve it. In Section 5, two specific graph fusion versions for multi-view spectral clustering are presented based on the proposed framework. Finally, we report the experimental results in Section 6 and conclude this paper in Section 7. More experimental results are reported in the Appendix.

2 RELATED WORK

In recent years, multi-view clustering has been a popular topic and many multi-view clustering algorithms have been developed from different technical perspectives.

Bickel and Scheffer [14] extended the semi-supervised co-training approaches [15] to multi-view clustering. The basic idea of co-training is to iterate over all views and optimize an objective function in next view using result obtained from last view. However, its limitation is that co-training based multi-view clustering algorithms may not converge [14] and thus it is difficult to decide when to stop.

Kumar et al. [16] proposed Co-regularized Spectral Clustering based on maximizing clustering agreement among all views. They presented an alternative regularization scheme that regularizes each view-specific set of eigenvectors towards a common centroid and used the common centroid to obtain the clustering result. The basic idea of their algorithm is that all views should yield a consensus clustering result. The idea of maximizing clustering agreement of all views is exploited by many other multi-view clustering approaches [17], [18], [19]. For example, Zong et al. [18] introduced Weighted Multi-View Spectral Clustering. They found that the similarity between the clustering results of different views can be measured by the largest canonical angle between the subspaces spanned by the eigenvectors

of the normalized Laplacian matrices for different views. Therefore, minimizing the canonical angles leads to maximizing the clustering agreement of all views. To eliminate the potential noise in data, Xia et al. [20] proposed Robust Multi-View Spectral Clustering, which aims to learn an intrinsic transition matrix from multiple views by restricting the transition matrix to be low-rank.

Nie et al. [21] use Procrustes Analysis technique to obtain a consensus cluster indicator matrix from the spectral embedding of multi-view kernels. One possible limitation to this approach is that some information of multi-view graphs is lost before obtaining the clustering result. To elaborate, we know that the eigenvectors corresponding to the largest eigenvalues of Laplacian matrix contain information to partition the graph [2]. The AWP method [21] use only information from the eigenvectors corresponding to some largest eigenvalues, and the information of the eigenvectors corresponding to other large eigenvalues is lost. To utilize the information from the entire spectrum of the Laplacian matrices of all views, it seems more reasonable to perform multi-view learning before obtaining spectral embedding. Our framework is likely to make the most of the spectral information in all views since the unified graph is learned before computing the eigenvectors.

Huang et al. [22] proposed a method for aggregating affinity matrices for spectral clustering, which attempts to reduce the influence of unreliable and irrelevant features in data. Nie et al. [10] proposed a parameter-free self-weighted scheme to fuse multiple graphs with the importance of each view considered. Zhan et al. [7], [8], [9] proposed to learn an intrinsic similarity graph from multiple similarity graphs. Their approaches learn the consensus graph by tuning the fused graph structure until it contains exactly the desired number of connected components n_c . During the iterative learning of graph structure, the n_c smallest eigenvalues of the graph Laplacian need to be computed. If there are exactly n_c smallest eigenvalues being 0, then the number of connected components is exactly n_c [4] and the learning is finished. However, with n_c eigenvalues being the same, which is termed eigenvalues cluster in the literature, the eigen-decomposition algorithm may have difficulty in converging [23]. As pointed out in [23], the closer the eigenvalues lie in the cluster, the slower the algorithm convergences [23]. Indeed, we have found in our experiments that the convergence of the MCGC [9] and MVGL [7] algorithms could be quite slow, which results in a heavy computational burden for larger datasets. Moreover, they mostly focus on the consistent properties across multiple views, but often lack the ability to simultaneously and explicitly model the multi-view inconsistency information, which may degrade their graph learning and clustering performances when faced with complex multi-view datasets.

3 LEARNING A CONSISTENT GRAPH WITH INCONSISTENCY CONSIDERED

In this section, we propose a new multi-view graph learning method which is capable of joint modeling of multi-view consistency and multi-view inconsistency in a unified optimization framework. The basic idea is to decompose the adjacency matrix of each graph (view) into two parts, the

1. https://github.com/youweiliang/Multi-view_Graph_Learning

consistent part and the inconsistent part. By the property of inconsistency, we design a novel objective function which can automatically identify the inconsistent parts and fuse the consistent parts into a unified adjacency matrix. By iteratively optimizing the objective function, the inconsistent and consistent parts of each view as well as the unified adjacency matrix are iteratively learned.

Let $\mathbf{W}^{(i)} \in \mathbb{R}_{\geq 0}^{n \times n}$ denotes the similarity matrix for the i -th view, with n being the number of instances (data points). The similarity matrices for different views may be significantly different even when they yield similar clustering results. For example, it is this case when $\mathbf{W}^{(i)} = k\mathbf{W}^{(j)}$. Then their symmetrically normalized Laplacian matrices $\mathbf{L}^{(i)} = \mathbf{L}^{(j)}$, which give exactly the same clustering results in normalized cut [3]. Therefore, we need to scale the similarity matrices before fusing them into a unified similarity matrix, i.e., multiplying $\mathbf{W}^{(i)}$ with a learnable scaling coefficient α_i . To make the scaling result unique, we restrict the sum of the coefficients to 1, i.e., $\alpha^\top \mathbf{1} = 1$. All the scaled similarity matrices should be close to the unified similarity matrix \mathbf{S} . Hence we want to minimize the following objective function with constraints:

$$\begin{aligned} \min_{\alpha, \mathbf{S}} \quad & \sum_{i=1}^v \left\| \alpha_i \mathbf{W}^{(i)} - \mathbf{S} \right\|_F^2 \\ \text{s.t.} \quad & \alpha^\top \mathbf{1} = 1, \alpha \geq 0, \mathbf{S} \geq 0. \end{aligned} \quad (1)$$

Here, v is the number of views.

To jointly model multi-view consistency and multi-view inconsistency, we decompose the similarity matrix $\mathbf{W}^{(i)}$ for the i -th view into two parts: the consistent part $\mathbf{A}^{(i)}$ and the inconsistent part $\mathbf{E}^{(i)}$. More formally, we assume that

$$\mathbf{W}^{(i)} = \mathbf{A}^{(i)} + \mathbf{E}^{(i)} \quad (2)$$

with $\mathbf{A}^{(i)}, \mathbf{E}^{(i)} \in \mathbb{R}_{\geq 0}^{n \times n}$. The core problem is how to find matrices $\mathbf{A}^{(i)}$ and $\mathbf{E}^{(i)}$ for $i = 1, \dots, v$.

Different from previous decomposition works [11], [20] that mainly focus on modeling the noise in data, in this paper, the concept of inconsistency in multi-view data includes not only noise, but also the difference in view-specific characteristics. While noise is typically considered sparse on a similarity graph [11], [20], the inconsistency may not. Since the relationship between data points may be intrinsically different across views, the inconsistency can appear everywhere on the similarity graphs. Thus, sparsity *within a similarity matrix* is no longer valid in identifying the inconsistency on multi-view similarity graphs. Instead, we assume that the inconsistency is sparse *across views*. For example, suppose we have five views and the similarities between data points x_1 and x_2 on each view are 3.16, 3.19, 3.22, 3.17, and 3.95, respectively (assuming we have properly scaled the similarity matrices). We tend to believe that a good similarity measure between x_1 and x_2 is 3.20 (i.e., the consistent part). The similarity on the 5-th view has a deviation of 0.75 (i.e., the inconsistent part) from the consistent part. We say the inconsistency is sparse across views because only the 5-th view has a relatively large inconsistent part. To ensure the inconsistency is sparse

across views, it is natural to make the sum of the products of the inconsistent parts to be a small value, i.e.,

$$\sum_{\substack{i,j=1 \\ i \neq j}}^v \text{sum} \left((\alpha_i \mathbf{E}^{(i)}) \circ (\alpha_j \mathbf{E}^{(j)}) \right), \quad (3)$$

where \circ denotes the Hadamard product (element-wise multiplication) of two matrices and $\text{sum}(\cdot)$ is the operator of summing all elements in a matrix. We scale the inconsistent part of each view to make them have fair contributions to the sum. Furthermore, we generally do not want the inconsistent parts to be too large, which leads to preventing the following value from becoming too large during learning:

$$\sum_{i=1}^v \text{sum} \left((\alpha_i \mathbf{E}^{(i)}) \circ (\alpha_i \mathbf{E}^{(i)}) \right). \quad (4)$$

To jointly model multi-view consistency and inconsistency in a unified optimization framework, we combine the three terms (1), (3) and (4) into one objective function:

$$\min_{\substack{\alpha, \mathbf{A}^{(1)}, \dots, \mathbf{A}^{(v)}, \\ \mathbf{E}^{(1)}, \dots, \mathbf{E}^{(v)}, \mathbf{S}}} \sum_{i=1}^v \left\| \alpha_i \mathbf{A}^{(i)} - \mathbf{S} \right\|_F^2 \quad (5)$$

$$+ \beta \sum_{i=1}^v \text{sum} \left((\alpha_i \mathbf{E}^{(i)}) \circ (\alpha_i \mathbf{E}^{(i)}) \right) \quad (6)$$

$$+ \gamma \sum_{\substack{i,j=1 \\ i \neq j}}^v \text{sum} \left((\alpha_i \mathbf{E}^{(i)}) \circ (\alpha_j \mathbf{E}^{(j)}) \right) \quad (7)$$

$$\begin{aligned} \text{s.t.} \quad & \alpha^\top \mathbf{1} = 1, \alpha \geq 0, \mathbf{S} \geq 0, \\ & \mathbf{W}^{(i)} = \mathbf{A}^{(i)} + \mathbf{E}^{(i)}, \\ & \mathbf{A}^{(i)} \geq 0, \mathbf{E}^{(i)} \geq 0, \quad i = 1, \dots, v, \end{aligned} \quad (8)$$

where β, γ are parameters, and β controls the magnitude of inconsistent parts and γ prevents the consistent parts being incorrectly moved to inconsistent parts (i.e., ensuring sparsity of multi-view inconsistency) as we now explain.

To see how this objective can remove multi-view inconsistency, let us consider the ideal case where all similarity matrices are consistent, it is easy to see the optimal value of objective (1) will be 0. In practice, however, it will not be 0 due to the inconsistency across views, and the higher the inconsistency, the larger the objective value. If the inconsistent parts are moved from the original similarity matrix $\mathbf{W}^{(i)}$ to the matrix $\mathbf{E}^{(i)}$, the first term (5) in the objective can be reduced to a small number, while the second term (6) will not increase much, since we can set β to a small number; the third term (7) will not increase much too, because inconsistency is sparse across views. Hence, the overall objective value will decrease. Therefore, *the optimization process is actually moving the inconsistent parts from the original similarity matrix $\mathbf{W}^{(i)}$ to the matrix $\mathbf{E}^{(i)}$ by minimizing the overall objective function*. This idea is the core principle of how we simultaneously model multi-view consistency and multi-view inconsistency in a unified optimization framework.

We shall transform the objective function to better apply optimization techniques. Let \mathbf{B} be a v -by- v matrix with its diagonal elements being β and off-diagonal elements being

γ . Then our objective function can be written in a more compact form

$$\begin{aligned} \min_{\substack{\alpha, \mathbf{S}, \\ \mathbf{A}^{(1)}, \dots, \mathbf{A}^{(v)}}} & \sum_{i=1}^v \lambda_i \left\| \alpha_i \mathbf{A}^{(i)} - \mathbf{S} \right\|_F^2 + \\ & \sum_{i,j=1}^v B_{ij} \lambda_i \lambda_j \alpha_i \alpha_j \text{sum} \left((\mathbf{W}^{(i)} - \mathbf{A}^{(i)}) \circ (\mathbf{W}^{(j)} - \mathbf{A}^{(j)}) \right) \\ \text{s.t. } & \alpha^\top \mathbf{1} = 1, \alpha \geq 0, \mathbf{S} \geq 0, \\ & \mathbf{W}^{(i)} \geq \mathbf{A}^{(i)} \geq 0, i = 1, \dots, v \end{aligned} \quad (9)$$

where λ_i is newly introduced to reflect the importance of the i -th view, and a higher value indicates greater importance. Normally users should set λ_i based on prior knowledge in the applications. If no such knowledge is available, we simply set $\lambda_i = 1$ for all $i \in \{1, \dots, v\}$. It is also possible that λ_i is learned by some algorithms, but we leave these for future works. The only requirement for λ_i is $\lambda_i > 0$ because negative value does not make sense and if $\lambda_i = 0$ we can simply remove the i -th view from the objective. The introduction of view-specific weights λ for multi-view learning adds flexibility to our framework. In our experiments, we set $\lambda_i = 1$ for all views.

4 OPTIMIZATION

Though the proposed framework has attractive features of identifying multi-view inconsistency and fusing consistent parts into a unified graph, the optimization of objective (9) is difficult for three reasons. Firstly, the objective function (9) is not jointly convex on all variables, which rules out the possibility of using convex optimization algorithms. Secondly, there are a lot of coupling between the variables, i.e., different variables are multiplied together, which causes the degree of the equation raised to the fourth. Thirdly and unfortunately, the optimization of objective (9) turns out to be NP-hard. In the preliminary version of this paper [12], a projection based method is applied to optimize the objective, which lacks the theoretical guarantee on convergence. Based on deeper theoretical understandings of the problem, we adopt the following approaches to tackle these problems. Firstly, by analyzing the constraints theoretically, we remove one of them that can be automatically satisfied. Secondly, our analysis of multi-view inconsistency issue largely simplifies the optimization, as we will discuss in Section 4.4.1. Furthermore, objective (9) can be rewritten as two forms of quadratic functions, corresponding to Subproblem (1) and Subproblem (3), so that we can optimize them alternately. Even so, Subproblem (3) consists of at least n nonconvex quadratic programs (QPs) with box constraints, which are difficult to solve since they are NP-hard [24]. By proving that these QPs share the same Hessian that has a desired property (Lemma 2), we are able to modify the d.c. algorithm [13] to solve them all at once, which is much more efficient than solving them sequentially. To facilitate these approaches, the multi-view dense representation is further proposed, where the nonzero elements of adjacency matrices of all views are arranged into one dense matrix.

4.1 Constraint Simplification

We first show that the constraint $\mathbf{S} \geq 0$ in Problem (9) can be removed while the global minimizer(s) remains the same. Define the following sets:

$$\mathcal{G}_0 = \{\alpha \geq 0 \mid \alpha^\top \mathbf{1} = 1\}, \quad (10)$$

$$\mathcal{G}_i = \{\mathbf{A}^{(i)} \mid \mathbf{W}^{(i)} \geq \mathbf{A}^{(i)} \geq 0\}, \quad i = 1, \dots, v, \quad (11)$$

$$\mathcal{G} = \mathcal{G}_0 \times \mathcal{G}_1 \times \dots \times \mathcal{G}_v \times \mathbb{R}^{n \times n}, \quad (12)$$

$$\mathcal{G}_+ = \mathcal{G}_0 \times \mathcal{G}_1 \times \dots \times \mathcal{G}_v \times \mathbb{R}_{\geq 0}^{n \times n}, \quad (13)$$

$$\mathcal{G}_- = \mathcal{G}_0 \times \mathcal{G}_1 \times \dots \times \mathcal{G}_v \times (\mathbb{R}^{n \times n} \setminus \mathbb{R}_{\geq 0}^{n \times n}), \quad (14)$$

where \times denotes the Cartesian product. Clearly, $\mathcal{G}_+, \mathcal{G}_- \subset \mathcal{G}$ and $\mathcal{G}_+ \cup \mathcal{G}_- = \mathcal{G}, \mathcal{G}_+ \cap \mathcal{G}_- = \emptyset$. Then objective function (9) is denoted by $f: \mathcal{G} \rightarrow \mathbf{R}$. The following lemma shows that with the constraint $\mathbf{S} \geq 0$ removed, the minimizer of the resulting problem still satisfies $\mathbf{S} \geq 0$.

Lemma 1. *For every minimizer x^* of the problem*

$$\min_x f(x), \quad \text{s.t. } x \in \mathcal{G}, \quad (15)$$

we have $x^ \in \mathcal{G}_+$.*

Proof: Suppose $x^* \notin \mathcal{G}_+$. Then $x^* \in \mathcal{G}_-$. Suppose $x^* = (\alpha, \mathbf{A}^{(1)}, \dots, \mathbf{A}^{(v)}, \mathbf{S})$, where $S_{pq} < 0$ for some $p, q \in \{1, \dots, n\}$. Let $\mathcal{V} = \{(p, q) \mid S_{pq} < 0\}$. Let $\tilde{x} = (\alpha, \mathbf{A}^{(1)}, \dots, \mathbf{A}^{(v)}, \tilde{\mathbf{S}}) \in \mathcal{G}_+$, where $\tilde{\mathbf{S}} \in \mathbb{R}_{\geq 0}^{n \times n}$ such that $\tilde{S}_{pq} = 0$ for all $(p, q) \in \mathcal{V}$ and $\tilde{S}_{pq} = S_{pq}$ for all $(p, q) \notin \mathcal{V}$. Let $c = \sum_{k=1}^v \lambda_k \sum_{(p,q) \notin \mathcal{V}} (\alpha_k A_{pq}^{(k)} - S_{pq})^2 + \sum_{i,j=1}^v B_{ij} \lambda_i \lambda_j \alpha_i \alpha_j \text{sum}((\mathbf{W}^{(i)} - \mathbf{A}^{(i)}) \circ (\mathbf{W}^{(j)} - \mathbf{A}^{(j)}))$. Then

$$\begin{aligned} f(x^*) &= f(\alpha, \mathbf{A}^{(1)}, \dots, \mathbf{A}^{(v)}, \mathbf{S}) \\ &= \sum_{k=1}^v \lambda_k \sum_{(p,q) \in \mathcal{V}} \left(\alpha_k A_{pq}^{(k)} - S_{pq} \right)^2 + c \\ &= \sum_{k=1}^v \lambda_k \sum_{(p,q) \in \mathcal{V}} \left(\left(\alpha_k A_{pq}^{(k)} \right)^2 + S_{pq}^2 - 2S_{pq} \alpha_k A_{pq}^{(k)} \right) + c \\ &> \sum_{k=1}^v \lambda_k \sum_{(p,q) \in \mathcal{V}} \left(\alpha_k A_{pq}^{(k)} \right)^2 + c \\ &= f(\tilde{x}). \end{aligned}$$

This contradicts that x^* is a minimizer of the problem (15). Therefore, we conclude that $x^* \in \mathcal{G}_+$. \square

Since the minimizer of Problem (15) cannot appear outside the region \mathcal{G}_+ , we do not need the constraint $\mathbf{S} \geq 0$, which largely simplifies the problem.

4.2 Optimization Scheme

Due to the high-order coupling of the variables, we adopt an alternating optimization scheme as follows. We first optimize the objective function over α with $\mathbf{S}, \mathbf{A}^{(1)}, \dots, \mathbf{A}^{(v)}$ fixed, and then over \mathbf{S} with $\alpha, \mathbf{A}^{(1)}, \dots, \mathbf{A}^{(v)}$ fixed, and then over $\mathbf{A}^{(1)}, \dots, \mathbf{A}^{(v)}$ with α and \mathbf{S} fixed. That is, we divide the problem into three subproblems and optimize one at a time. We repeat the procedures until the objective value converges. The objective (9) can be rewritten as two

different forms, (17) and (18), which show that it is actually quadratic forms of $\{\alpha_i\}$ in (17) or $\{A_{jk}^{(i)}\}$ in (18).

$$f(\alpha, \mathbf{A}^{(1)}, \dots, \mathbf{A}^{(v)}, \mathbf{S}) = \sum_{i=1}^v \lambda_i \sum_{j,k} (\alpha_i A_{jk}^{(i)} - S_{jk})^2 + \quad (16)$$

$$\sum_{i,l=1}^v B_{il} \lambda_i \lambda_l \alpha_i \alpha_l \sum_{j,k} (W_{jk}^{(i)} - A_{jk}^{(i)}) (W_{jk}^{(l)} - A_{jk}^{(l)})$$

$$= \sum_{i=1}^v \left(\lambda_i \sum_{j,k} (A_{jk}^{(i)})^2 \right) \alpha_i^2 - 2 \sum_{i=1}^v \left(\lambda_i \sum_{j,k} A_{jk}^{(i)} S_{jk} \right) \alpha_i + \quad (17)$$

$$\sum_{i,l=1}^v \left(B_{il} \lambda_i \lambda_l \sum_{j,k} (W_{jk}^{(i)} - A_{jk}^{(i)}) (W_{jk}^{(l)} - A_{jk}^{(l)}) \right) \alpha_i \alpha_l + C_1$$

$$= \sum_{j,k} \left[\sum_{i=1}^v \lambda_i \alpha_i^2 (A_{jk}^{(i)})^2 + \sum_{i,l=1}^v B_{il} \lambda_i \lambda_l \alpha_i \alpha_l A_{jk}^{(i)} A_{jk}^{(l)} - \right. \quad (18)$$

$$\left. 2 \sum_{i=1}^v \left(\lambda_i \alpha_i S_{jk} + \sum_{l=1}^v B_{il} \lambda_i \lambda_l \alpha_i \alpha_l W_{jk}^{(i)} \right) A_{jk}^{(i)} \right] + C_2$$

where C_1 is a quantity which does not depend on α , and C_2 is a quantity which does not depend on $\mathbf{A}^{(1)}, \dots, \mathbf{A}^{(v)}$. Let $q(\alpha) = f(\alpha, \mathbf{A}^{(1)}, \dots, \mathbf{A}^{(v)}, \mathbf{S}) - C_1$, i.e., the first two terms of (17), and $p(\mathbf{A}^{(1)}, \dots, \mathbf{A}^{(v)}) = f(\alpha, \mathbf{A}^{(1)}, \dots, \mathbf{A}^{(v)}, \mathbf{S}) - C_2$, i.e., the first terms in (18). Then Subproblem (1) is to optimize $q(\alpha)$ w.r.t. α and Subproblem (3) is to optimize $p(\mathbf{A}^{(1)}, \dots, \mathbf{A}^{(v)})$.

4.3 Multi-view Dense Representation

In the preliminary version of this paper [12], the optimization is performed on sparse matrices, but we discover that it is a better approach to construct a dense matrix with the nonzero elements from the sparse matrices of all views, from the perspectives of both time and memory efficiency.

Since there are typically a lot of zero elements in the multi-view (sparse) adjacency matrices $\mathbf{W}^{(i)}$, many terms within the summation in (17) and (18) vanish. Let \mathcal{F} be the common index set of the nonzero elements in the adjacency matrices of all views. We form v row vectors by taking the elements from $\mathbf{W}^{(1)}, \dots, \mathbf{W}^{(v)}$, corresponding to the indices in \mathcal{F} , and then stack the row vectors to form a v -by- n_d matrix \mathbf{W} (note the notation difference from $\mathbf{W}^{(i)}$), where n_d is the number of elements in \mathcal{F} . Similarly, we form a v -by- n_d matrix \mathbf{A} from $\mathbf{A}^{(1)}, \dots, \mathbf{A}^{(v)}$. Then the inconsistent part for all views is $\mathbf{E} = \mathbf{W} - \mathbf{A}$ and the fused graph is represented by a row vector \mathbf{s} of length n_d . Multi-view dense representation is more efficient than sparse matrix representation, since the latter requires as three times storage as the former and it is faster to access elements in a dense matrix than in a sparse one. For these reasons we use only multi-view dense representation in our optimization algorithm.

It is recommended that the multi-view adjacency matrices should be normalized before performing optimization algorithm because normalization aids the optimization process and can reduce the total number of iterations. A typical normalization method is dividing the (non-negative) adjacency matrices by its sum or Frobenius norm. For the multi-view dense representation \mathbf{W} , we normalize each row individually.

4.4 Subproblem (1)

With \mathbf{A} and \mathbf{s} fixed, we optimize $q(\alpha)$. Note that $q(\alpha)$ is a quadratic function of α . Formally it is formulated as a quadratic program (QP) on simplex (Subproblem (1)) [25]:

$$\min_{\alpha} \quad q(\alpha) = 1/2 \alpha^\top \mathbf{H} \alpha - \alpha^\top \mathbf{c} \quad (19)$$

$$\text{s.t.} \quad \alpha^\top \mathbf{1} = 1, \alpha \geq 0 \quad (20)$$

where \mathbf{H} and \mathbf{c} are computed by (17) as we now explain. Let \mathbf{h} be a vector (of length v) by taking the squared ℓ_2 norm of each row of \mathbf{A} , and let \mathbf{T} be a v -by- v diagonal matrix by placing the vector $\lambda \circ \mathbf{h}$ on the diagonal. Let \mathbf{Z} and \mathbf{P} be v -by- v matrices defined as $Z_{ij} = B_{ij} \lambda_i \lambda_j$ and $\mathbf{P} = \mathbf{Z} \circ (\mathbf{E} \mathbf{E}^\top)$ where $\mathbf{E} = \mathbf{W} - \mathbf{A} \in \mathbb{R}^{v \times n_d}$ is the inconsistent parts for all views. According to (17), the Hessian of $q(\alpha)$ is $\mathbf{H} = 2(\mathbf{T} + \mathbf{P})$. By (17), the linear coefficient of $q(\alpha)$ can be defined as $c_i = 2\lambda_i \mathbf{A}_i \mathbf{s}^\top$ where \mathbf{A}_i is the i -th row of \mathbf{A} .

4.4.1 Multi-view Inconsistency Indicator

The QP in Subproblem (1) has an inequality constraint $\alpha \geq 0$ and the Hessian \mathbf{H} can be indefinite. Since we do not know for which α_i the equality $\alpha_i = 0$ holds, the problem is essentially a combinatorial problem [26], [27], which greatly increases the difficulty of solving it. Fortunately, our analysis shows that the inequality constraint can be removed under a reasonable assumption as we now explain. If we assume the multi-view matrices \mathbf{W}_i are nearly consistent with each other, then we can remove the constraint $\alpha \geq 0$ in (20) without worrying it would be violated. To elaborate, if the inconsistency is small across views, the scaled adjacency matrices of all views $\alpha_i \mathbf{A}^{(i)}$ is close to the unified adjacency matrix \mathbf{S} . Since we have constraint $\sum_{i=1}^v \alpha_i = 1$, then in the optimal solution α there must exist j such that $\alpha_j > 0$ even if constraint $\alpha \geq 0$ is removed. Thus, $\alpha_j \mathbf{A}^{(j)} \geq 0$ and $\mathbf{S} \geq 0$. Then the other views $\alpha_i \mathbf{A}^{(i)} \geq 0$ since they are close to \mathbf{S} (by our consistency assumption) and thus the other $\alpha_i \geq 0$. In summary, if the multi-view inconsistency is small, then the inequality constraint $\alpha \geq 0$ can be automatically satisfied and thus can be removed from the constraints. In practice the inconsistency across views is generally not very large, then we can try to solve Subproblem (1) without constraint $\alpha \geq 0$. If the resulting solution violates the constraint, we can use the active set algorithm [25] to solve the problem again with the constraint. This approach greatly improves the efficiency since it is much faster to solve Subproblem (1) without constraint $\alpha \geq 0$.

Our analysis shows that multi-view consistency is correlated to the sign of α when we solve Subproblem (1) without constraint $\alpha \geq 0$ (see (23) in Section 4.4.2 for the solution). If in the solution to (23), $\alpha_i \leq 0$ for some i , then there is a view that is largely inconsistent with other views. Therefore, we may use the sign of α_i as an indicator of large multi-view inconsistency. Besides, note that the (i, j) -th element of $\mathbf{E} \mathbf{E}^\top$ equals $\text{sum}(\mathbf{E}^{(i)} \circ \mathbf{E}^{(j)})$, and thus with proper scaling, i.e., multiplying $\alpha_i \alpha_j$, it becomes the inconsistency between the i -th view and j -th view. Therefore, the matrix $\hat{\mathbf{E}} = (\alpha \alpha^\top) \circ (\mathbf{E} \mathbf{E}^\top)$, termed multi-view inconsistency matrix, represents the inconsistency of all views.

4.4.2 Solving Subproblem (1) via Linear Equations

Without constraint $\alpha \geq 0$, we can solve the problem with a Lagrangian function $\mathcal{L}(\alpha, \mu) = 1/2 \alpha^\top \mathbf{H} \alpha - \alpha^\top \mathbf{c} + \mu(\alpha^\top \mathbf{1} - 1)$. The first order optimality conditions are

$$\frac{\partial \mathcal{L}}{\partial \alpha} = \mathbf{H} \alpha - \mathbf{c} + \mu \mathbf{1} = \mathbf{0}, \quad (21)$$

$$\alpha^\top \mathbf{1} = 1. \quad (22)$$

Note that (21) and (22) can be written in one equation:

$$\begin{bmatrix} \mathbf{H} & \mathbf{1} \\ \mathbf{1}^\top & 0 \end{bmatrix} \cdot \begin{bmatrix} \alpha \\ \mu \end{bmatrix} = \begin{bmatrix} \mathbf{c} \\ 1 \end{bmatrix}. \quad (23)$$

Then we can solve the system of linear equations for α . When solving Eq. (23), we can safely assume the coefficient matrix is non-singular. This is because the inconsistent parts are typically random, and thus the coefficient matrix is very likely to be non-singular [28]. In fact, we have never encountered any singular coefficient matrix in our experiments. Besides, we have found in our experiments that the α obtained from Eq. (23) is non-negative in most cases (more than 99%). If we obtain negative α_i from Eq. (23), we can switch to the active set algorithm in [25] that solves QPs with simplex constraints.

4.5 Subproblem (2)

In this section we update \mathbf{s} with α and \mathbf{A} fixed. Taking the derivative of objective function (9) with respect to \mathbf{S} gives

$$2\left(\sum_{i=1}^v \lambda_i\right) \mathbf{S} - 2 \sum_{i=1}^v \lambda_i \alpha_i \mathbf{A}^{(i)} = \mathbf{0}.$$

Thus,

$$\mathbf{S} = \sum_{i=1}^v (\lambda_i \alpha_i \mathbf{A}^{(i)}) / \left(\sum_{i=1}^v \lambda_i\right). \quad (24)$$

In multi-view dense representation, (24) becomes

$$\mathbf{s} = \mathbf{t}^\top \mathbf{A} \quad (25)$$

where $\mathbf{t} = \lambda \circ \alpha / (\sum_{i=1}^v \lambda_i)$.

4.6 Subproblem (3)

In this section we update \mathbf{A} with α and \mathbf{s} fixed. For a pair of fixed (j, k) , let $\mathbf{a} = [A_{jk}^{(1)}, \dots, A_{jk}^{(v)}]^\top$ be the corresponding column of \mathbf{A} . Then the three terms within the brackets in (18) is a quadratic function of \mathbf{a} , for which we can formulate a quadratic program (QP) with upper and lower bound:

$$\min_{\mathbf{a}} \quad 1/2 \mathbf{a}^\top \mathbf{D} \mathbf{a} - \mathbf{l}^\top \mathbf{a} \quad (26)$$

$$\text{s.t.} \quad \mathbf{0} \leq \mathbf{a} \leq \mathbf{u} \quad (27)$$

where $\mathbf{u} = [W_{jk}^{(1)}, \dots, W_{jk}^{(v)}]^\top$ is the corresponding column of \mathbf{W} , and \mathbf{D} and \mathbf{l} is computed by (18) as we soon explain. For now, we need to solve a quadratic program for every pair of (j, k) . Fortunately, note that in (18), summing over (j, k) is the same as summing over the indices of nonzero elements in $\mathbf{A}^{(i)}$. Since the adjacency matrices are usually sparse, the actual number of quadratic programs (QPs) we need to solve is n_d instead of n^2 , where n_d is the number of elements in \mathcal{F} (see Section 4.3). For example, when k NN graphs are used to construct similarity graphs, the number

of QPs is $n_d = kn$, where k is the number of nearest neighbors and n is the number of data points. In multi-view dense representation, every column of \mathbf{A} corresponds to a QP. Fortunately, these QPs share the same Hessian \mathbf{D} as we can see in (18). With this observation, we find that Subproblem (3) can be efficiently solved via the d.c. (difference of convex functions) optimization algorithms [13], which requires only matrix multiplication and is simple to implement. Since the original d.c. algorithm (DCA) solves only one QP at a time, we modify it so that it can efficiently solve multiple QPs with same Hessian all at once, as presented in Algorithm 1. To do so, we need to combine the linear coefficients of these QPs by stacking all l (column vectors) of each QP horizontally to form a v -by- n_d matrix \mathbf{L} , and the combined lower bound and upper bound of the QPs are $\mathbf{0}$ and \mathbf{W} , respectively.

To compute \mathbf{D} and \mathbf{L} , let \mathbf{K} be a v -by- v matrix defined as $K_{ij} = B_{ij} \lambda_i \lambda_j \alpha_i \alpha_j$. Let \mathbf{Q} be a v -by- v diagonal matrix defined as $Q_{ii} = \lambda_i \alpha_i^2$. According to (18), the Hessian of all QPs is $\mathbf{D} = 2(\mathbf{Q} + \mathbf{K})$. Let $\mathbf{t} = \lambda \circ \alpha$ and $\mathbf{P} = \mathbf{t} \circ \mathbf{s}$ where the second \circ is broadcasting element-wise multiplication, i.e., $P_{ij} = t_i s_j$. The combined linear coefficient of all QPs is $\mathbf{L} = 2(\mathbf{P} + \mathbf{K}\mathbf{W})$. In Algorithm 1, we need to compute ρ , the largest eigenvalue of \mathbf{D} , which is required to be positive [13]. Fortunately, this requirement is satisfied as shown in the following lemma.

Lemma 2. *The matrix \mathbf{D} has at least one positive eigenvalue.*

Proof: By the definition of \mathbf{D} , for all $1 \leq i \leq v$, $D_{ii} = 2(Q_{ii} + K_{ii})$ where $Q_{ii} = \lambda_i \alpha_i^2$ and $K_{ii} = B_{ii} \lambda_i^2 \alpha_i^2$. Since $B_{ii} \geq 0$ and $\lambda_i > 0$ by our definitions, then $Q_{ii} \geq 0$ and $K_{ii} \geq 0$. Note that for all $i \in \{1, \dots, v\}$, $\alpha_i \geq 0$ and $\sum_{i=1}^v \alpha_i = 1$ by constraints (20). Thus, there exists $j \in \{1, \dots, v\}$ such that $\alpha_j > 0$. Then $Q_{jj} > 0$ and thus $D_{jj} > 0$. Suppose \mathbf{D} is negative semi-definite. Then for any vector $\mathbf{v} \in \mathbb{R}^v$, $\mathbf{v}^\top \mathbf{D} \mathbf{v} \leq 0$. If we let $\mathbf{v} = \mathbf{e}_j$, where $\mathbf{e}_j \in \mathbb{R}^v$ is the j -th unit vector (i.e., its j -th element is 1 and all other elements is 0), then $\mathbf{e}_j^\top \mathbf{D} \mathbf{e}_j = D_{jj} > 0$. This leads to a contradiction and thus \mathbf{D} is not negative semi-definite. Then \mathbf{D} has at least one positive eigenvalue. \square

Another reason to use DCA is that \mathbf{D} can be indefinite, which can be seen by adjusting β , γ and λ . Consequently, the QPs in Subproblem (3) are nonconvex and thus solving them is NP-hard [24], while DCA is designed for such nonconvex QPs [13].

Algorithm 1 Parallelized DCA for Quadratic Programs with box constraints (modified Algorithm 2a in [13])

Input: \mathbf{D} (Hessian), \mathbf{L} (combined linear coefficient), \mathbf{W} (upper bound), \mathbf{A} (initial point), N (number of iterations)

Output: \mathbf{A}

- 1: Compute ρ , the largest eigenvalue of \mathbf{D} .²
- 2: $\mathbf{H} \leftarrow \rho \mathbf{I} - \mathbf{D}$ $\triangleright \mathbf{I} \in \mathbb{R}^{v \times v}$ is an identity matrix
- 3: **for** $i = 1, \dots, N$ **do**
- 4: $\mathbf{Y} \leftarrow \mathbf{H} \mathbf{A}$
- 5: $\mathbf{A} \leftarrow (\mathbf{Y} + \mathbf{L}) / \rho$
- 6: $\mathbf{A} \leftarrow \text{mid}(0, \mathbf{A}, \mathbf{W})$
- 7: **end for**

2. This can be done with Implicit Restarted Lanczos Method [29].

In Algorithm 1, $\text{mid}(\cdot, \cdot, \cdot)$ denotes element-wise median operator, i.e., the (i, j) -th element of $\text{mid}(0, \mathbf{A}, \mathbf{W}) = \min(\max(0, A_{ij}), W_{ij})$. We found that Algorithm 1 converges very fast, usually in 3 iterations, as pointed out in [13]. Thus, $N = 3$ is a default choice.

4.7 Consistent Graph Learning Algorithm

By alternatively solving the three subproblems, objective (9) is optimized and the inconsistent part of each view is removed and the unified adjacency matrix of all view is iteratively learned. The complete consistent graph learning algorithm is presented in Algorithm 2.

Since Subproblem (3) is already NP-hard, finding a global minimizer of objective (9) is also NP-hard. When solving Subproblems (1) and (2), the objective always decreases [26]. In Subproblem (3) the objective is guaranteed to decrease if the global DCA algorithm in [13] is applied. For efficiency reason, the local DCA is used and the objective can almost surely decrease [13]. Since objective (9) is bounded below by 0, the algorithm can converge and a local minimizer can be found. As a rule of thumb, we consider Algorithm 2 converges if the reduction of the objective value in an iteration is less than 1% of the total objective reduction.

Algorithm 2 Consistent Graph Learning

Input: Adjacency matrices $\{\mathbf{W}^{(1)}, \dots, \mathbf{W}^{(v)}\}$, β , γ , λ , M (max iteration)

Output: Adjacency matrix of the unified graph \mathbf{S}

- 1: Construct multi-view dense representation \mathbf{W} ; normalize \mathbf{W} ; initialize $\mathbf{A} = \mathbf{W}$, $\alpha = 1/v$, set s with Eq. (25)
 - 2: **repeat**
 - 3: Obtain α by solving Eq. (23)
 - 4: **if** $\alpha \notin \mathbb{R}_{\geq 0}^v$ **then**
 - 5: use the active set algorithm [25] to recompute α
 - 6: **end if**
 - 7: Update s with Eq. (25)
 - 8: Use Algorithm 1 to update \mathbf{A}
 - 9: **until** convergence or max iteration is reached
 - 10: Construct \mathbf{S} with s according to the index set \mathcal{F}
-

4.7.1 Complexity Analysis

In Subproblem (1), we compute the Hessian \mathbf{H} and linear coefficient \mathbf{c} of a QP, which requires $O(v^2 n_d)$ time and $O(v(v + n_d))$ space. Solving the QP via linear equations requires $O(v^3)$ time and $O(v^2)$ space. If the active set algorithm (ASA) [25] is used, the projection step in ASA requires $O(v \log v)$ time and $O(v)$ space, and the conjugate gradient step requires $O(v^3)$ time and $O(v^2)$ space [25]. Thus, solving the QP via ASA requires $O(m_1 v^3)$ time and $O(v^2)$ space, where m_1 is the number of iterations in ASA. Thus, solving Subproblem (1) requires $O(v^2(m_1 v + n_d))$ time and $O(v(v + n_d))$ space. Solving Subproblem (2) requires $O(v n_d)$ time and $O(v n_d)$ space. In Subproblem (3), computing \mathbf{D} and \mathbf{L} requires $O(v^2 n_d)$ time and $O(v(v + n_d))$ space. Computing the largest eigenvalue ρ of \mathbf{D} requires $O(v^2 \kappa(\mathbf{D}))$ time and $O(v^2)$ space [30], where $\kappa(\mathbf{D})$ is the condition number of \mathbf{D} . Then Algorithm 1 requires $O(v^2 n_d)$ time and $O(v(v + n_d))$ space. Thus, the total time complexity is $O(m_2 v^2(v m_1 + \kappa(\mathbf{D}) + n_d))$, where m_2 is the number of

iterations of the loop in Algorithm 2, and the total space complexity is $O(v(v + n_d))$. In practice, we solve Subproblem (1) via linear equations in most cases, and we found that m_2 is typically less than 10 in our experiments (see Figure 2). Under these conditions, we expect the running time of Algorithm 2 to be $O(v^2(v + \kappa(\mathbf{D}) + n_d))$. Assuming $n_d \gg v$ and $n_d \gg \kappa(\mathbf{D})$, the complexity reduces to $O(v^2 n_d)$, which means that the running time is basically linear in the number of edges n_d and quadratic in the number of views v . Since $n_d = kn$ in k NN graphs where k is the number of nearest neighbors and n is the number of data points, the time complexity further reduces to $O(knv^2)$.

5 TWO GRAPH FUSION VERSIONS

The proposed multi-view graph learning method is applicable to both similarity graphs and distance (dissimilarity) graphs. Thus, we extend our multi-view clustering framework into two graph fusion versions, Similarity Graph Fusion (SGF) and Distance Graph Fusion (DGF). The reason to fuse distance matrix is that distance may better reflect the relationship between data points than similarity as we soon explain in Section 5.2.

5.1 Similarity Graph Fusion

Similarity Graph Fusion (SGF) fuses multiple similarity graphs into one. If full similarity graphs are available, we first construct k NN similarity graphs, which means only the edges connecting a node and its k -nearest neighbors are kept on the similarity graph [4]. It is worth noting that the k NN graphs used in our algorithms are slightly different from the usual ones. The difference is that, when constructing the k NN graph for a view, we keep the edge connecting nodes x_i and x_j if x_i is among the k -nearest neighbors of x_j in *any* view. Then the positions (i.e., the index set \mathcal{F}) of nonzero elements in the similarity matrices for all views will be the same, and we use them to construct the multi-view dense representation. Note that this will cause the number of nonzero elements in each row of the learned unified matrix greater than k . We can select the k NN for each node after learning the unified graph.

As k NN captures the local structure by preserving the edges of the nearest neighbors, we further normalize these edges in k NN distance graphs and strengthen a small portion of strong edges (associated with low distance) from a global perspective *before* learning the unified graph. Let \mathbf{D} be the edges in k NN distance graphs, and let $\mu = \text{mean}(\mathbf{D})$, $\sigma = \text{std}(\mathbf{D})$ be the mean and standard deviation of these edges, respectively. Without loss of generality, the edges that are 1σ lower than the mean distance are considered the strong edges and will be set to zero. Mathematically, the normalization for k NN graph is

$$\mathbf{D} = \max((\mathbf{D} - \mu + \sigma)/\sigma, 0) = \max((\mathbf{D} - \mu)/\sigma + 1, 0), \quad (28)$$

where all operations are element-wise. Note that the distance of 0 will be transformed to the maximum similarity of 1 by means of the Gaussian kernel mapping and hence the strong edges that are set to 0 are “strengthened”. More importantly, the normalization of k NN graphs provides a baseline for the graph learning algorithm to compare

edges from multiple views with different mean and different standard deviations, which aids the process of fusing them into one unified graph.

Lastly, we perform spectral clustering on the final unified graph to obtain the clustering results. The Similarity Graph Fusion algorithm for spectral clustering is summarized in Algorithm 3.

Algorithm 3 Similarity Graph Fusion for Spectral Clustering

Input: Dataset with v views $\mathcal{X} = \{\mathbf{X}^{(1)}, \dots, \mathbf{X}^{(v)}\}$, number of clusters n_c , β, γ (for Algorithm 2), k (number of k NN)

Output: Cluster indicator vector \mathbf{c}

- 1: Construct k NN distance graphs $\{\mathbf{W}^{(1)}, \dots, \mathbf{W}^{(v)}\}$ that share neighbors across views
 - 2: Normalize each k NN graph and strengthen the strong edges with Eq. (28)
 - 3: Apply Gaussian kernel function to transform k NN distance graphs to k NN similarity graphs
 - 4: Use Algorithm 2 to obtain the unified similarity matrix \mathbf{S} from the k NN similarity graphs
 - 5: Keep the k largest elements at each row of \mathbf{S} and set other elements to 0
 - 6: $\mathbf{S} \leftarrow (\mathbf{S} + \mathbf{S}^\top)/2$
 - 7: Perform spectral clustering on \mathbf{S} to obtain cluster indicator vector \mathbf{c}
-

5.2 Distance (Dissimilarity) Graph Fusion

Distance (Dissimilarity) Graph Fusion (DGF) learns the unified graph directly from multiple distance (dissimilarity) graphs, since fusion of distance may better preserve the relationship between nodes than the fusion of similarity. We know that distance is transformed to similarity with a kernel (similarity) function, typically with the Gaussian kernel $k(\mathbf{x}_i, \mathbf{x}_j) = \exp(- (d(\mathbf{x}_i, \mathbf{x}_j))^2 / (2\rho^2))$ where $d(\mathbf{x}_i, \mathbf{x}_j)$ is the distance between \mathbf{x}_i and \mathbf{x}_j under some metric. The kernel function may bias the intrinsic relationship between nodes in the original graphs and exert a negative influence on the consistent graph learning process. Therefore, we suggest directly learning a unified graph from the distance (dissimilarity) graphs of all views. Then we apply a kernel (similarity) function to the learned unified graph to transform distance to similarity. That is, line 3 and line 4 in Algorithm 3 become

-
- 3: Use Algorithm 2 to obtain the unified distance matrix from the k NN distance graphs
 - 4: Apply Gaussian kernel function to transform the unified distance graph to unified similarity graph \mathbf{S}
-

A natural question in practice is how to measure the distance (dissimilarity) between data points (nodes). A widely used metric is Euclidean distance while the choice largely depends on the applications. If the features are words frequency, the cosine distance is more suitable than Euclidean distance and it is calculated as $d(\mathbf{x}_i, \mathbf{x}_j) = 1 - \mathbf{x}_i^\top \mathbf{x}_j / (\|\mathbf{x}_i\| \|\mathbf{x}_j\|)$.

6 EXPERIMENTS

We perform extensive experiments to compare the two proposed graph learning-based multi-view spectral clustering

TABLE 1
Statistics of the real-world datasets

| Dataset | # views | # classes | # instances |
|---------------|---------|-----------|-------------|
| ORL | 3 | 40 | 400 |
| Yale | 3 | 15 | 165 |
| Reuters | 5 | 6 | 1200 |
| BBCSport | 2 | 5 | 544 |
| NUS-WIDE | 5 | 31 | 2000 |
| Reuters-21578 | 5 | 6 | 1500 |
| MSRC-v1 | 5 | 7 | 210 |
| CiteSeer | 2 | 6 | 3312 |
| ALOI | 4 | 100 | 10800 |
| Flower17 | 7 | 17 | 1360 |
| Caltech101 | 6 | 102 | 9144 |
| UCI Digits | 6 | 10 | 2000 |

algorithms, namely SGF and DGF, against seven state-of-the-art multi-view spectral clustering algorithms, namely, Co-Regularized Spectral Clustering (CoReg) [16], Robust Multi-view Spectral Clustering (RMSC) [20], Affinity Aggregation for Spectral Clustering (AASC) [22], Weighted Multi-view Spectral Clustering based on spectral perturbation (WMSC) [18], multi-view clustering via Adaptively Weighted Procrustes (AWP) [21], Graph Learning for Multi-view Clustering (MVGL) [7], and Multi-view Consensus Graph Clustering (MCGC) [9]. In addition, the conventional Spectral Clustering (SC) [3] is also performed on each view of the datasets, and the best single-view SC performance is reported.

6.1 Datasets and Evaluation Metrics

Except the datasets used in the preliminary version of this paper, we conduct experiments on more datasets in this paper, with a total of 12 datasets as we now introduce. The ORL dataset contains 400 face images of 40 distinct subjects.³ The Yale dataset contains 165 gray-scale images of 15 individuals.⁴ The Reuters dataset contains 1200 documents, where each document is in 5 languages (views).⁵ The BBCSport dataset consists of 544 documents from the BBC Sport website.⁶ The NUS-WIDE dataset contains multi-view features extracted from images of the NUS-WIDE-OBJECT dataset reported in [31]. The Reuters-21578 dataset is a collection of documents that appeared on Reuters news in 1987.⁷ The MSRC-v1 dataset [32] contains 240 pixel-wise labeled images. The CiteSeer dataset contains 3312 documents.⁸ The ALOI dataset⁹ is a collection of 110250 images of 1000 small objects [33]. Since it is too large for some algorithms such as CoReg and RMSC, we follow Houle et al. [34] to use a subset. The Flower17 dataset consists of images of 17 categories of flower¹⁰, and the multi-view features are extracted by Nilsback and Zisserman [35], [36]. The Caltech101 dataset contains pictures of objects belonging

3. <http://cam-orl.co.uk/facedatabase.html>

4. <http://cvc.cs.yale.edu/cvc/projects/yalefaces/yalefaces.html>

5. <http://lig-membres.imag.fr/grimal/data.html>

6. <http://mlg.ucd.ie/datasets/segment.html>

7. <https://archive.ics.uci.edu/ml/datasets/reuters-21578+text+categorization+collection>

8. <http://lig-membres.imag.fr/grimal/data.html>

9. https://elki-project.github.io/datasets/multi_view

10. <http://www.robots.ox.ac.uk/~vgg/data/flowers/17/>

to 101 categories.¹¹ The UCI Digits dataset contains 2000 images of handwritten digits.¹² The statistics of the datasets are summarized in Table 1 and more details of these datasets can be found in the Appendix.

The normalized mutual information (NMI) [37], adjusted rand index (ARI) [38], clustering accuracy (ACC) [9] and purity [9] are used to measure the clustering performance.

6.2 Experimental Setup

We downloaded the source code of AWP, AASC, MVGL and MCGC from the authors' websites, and implement other algorithms following the instruction in the original papers. We conduct all experiments with MATLAB R2019b on a machine with an Intel Core i9-9960X 16-core CPU and 128GB RAM. For the algorithms which use the Laplacian matrices of graphs, we adopt the symmetrically normalized Laplacian $\mathbf{L}_{sym} = \mathbf{I} - \mathbf{D}^{-1/2}\mathbf{S}\mathbf{D}^{-1/2}$, where \mathbf{S} and \mathbf{D} are the adjacency matrix and degree matrix of the graph, respectively [3], [4]. We fix the number of the nearest neighbors in k NN to 6 in all experiments. For the algorithms with parameter(s), which include CoReg (1 parameter), RMSC (1 parameter), MCGC (1 parameter), WMSC (2 parameters), DGF and SGF (2 parameters), we use grid search to test the parameter(s) of these algorithms on the grids $\{10^{-5}, 10^{-4}, \dots, 10^5\}^m$, where m is the number of parameters of the algorithm, and we report the scores with the best parameter(s) (i.e., the parameter(s) achieving the highest NMI) found on each dataset. Note that the grids contain values that are very close to the parameters suggested by the authors. Thus, all algorithms should exhibit their best performance in the experiments. We set the weights λ_i for each view to 1 in DGF and SGF, without considering the importance of different views.

We run all algorithms 10 times and report the average scores and standard deviation. If k -means clustering is used in any algorithm, we run k -means 10 times and set its maximum number of iterations to 1000 to reduce the effect of random initialization. We use cosine distance to construct distance matrices for the text datasets Reuters, Reuters-21578, BBCSport and CiteSeer, and use Euclidean distance for other datasets. All distance matrices are transformed to similarity matrices with the Gaussian kernel. The parameter ρ in Gaussian kernel is set to the mean value of the edges in the k NN distance graph.

6.3 Clustering Result

The clustering performance is shown in Table 2. We can see that multi-view clustering methods generally achieve better performance than single-view clustering. The two proposed graph learning methods, DGF and SGF, achieve better performance than other state-of-the-art methods on most datasets in the experiments, which demonstrates the effectiveness and robustness of the proposed algorithms. Our algorithms outperform RMSC, which is another multi-view clustering method that is robust to noise, as we model not only noise but also the multi-view inconsistency in our framework. Besides, the graph learning methods AASC,

MVGL and MCGC do not outperform our methods probably because they neglect the inconsistency across views in graph learning. We also note that DGF seems to perform more robustly than SGF (e.g., in MSRC-v1 and Caltech101), whose reason might be our hypothesis in Section 5.2 that fusion of distance matrices may better preserve the relationship between data points (or nodes).

It is noteworthy that, even without dataset-specific parameter tuning, the proposed algorithms can still achieve stably high-quality clustering results in the benchmark datasets as indicated by the parameter analysis in Section 6.5. Thereby, we fix the parameters of DGF and SGF by setting $\beta = 1$ and $\gamma = 10^4$ and run the two algorithms on the 12 datasets. The result is that DGF and SGF with fixed parameters still outperform the state-of-the-art multi-view clustering methods on most datasets. Please see the Appendix for the experimental results.

6.4 Convergence Analysis

We propose an alternating minimization scheme to solve the optimization problem in the proposed graph learning framework by dividing it into three subproblems. If the global DCA in [13] is exploited to solve Subproblem (3), the objective function is guaranteed to converge. For efficiency reasons, we only apply the local DCA [13] to Subproblem (3), which almost surely converges [13]. In our hundreds of experiments under different parameters on various datasets, the optimization algorithm with local DCA always converges, mostly within a few iterations, which demonstrates its reliability and efficiency. The convergence curves are shown in Figure 2.

6.5 Parameters Sensitivity

We have two parameters β and γ in the proposed multi-view graph learning algorithm. We test (β, γ) on the grid $\{10^{-5}, 10^{-4}, \dots, 10^5\} \times \{10^{-5}, 10^{-4}, \dots, 10^5\}$. The result is shown in Figure 3, which demonstrates that the performance of the proposed framework is stable across a wide range of parameters. We emphasize that even without parameter tuning, the framework still achieves generally superior performance against the state of the art. Please see the Appendix for the experiments.

6.6 Algorithmic Efficiency

We record the running time of each algorithm and report the results in Table 3. We can see that DGF and SGF are among the two fastest multi-view algorithms on some datasets and run comparably fast on the other datasets against other algorithms. Moreover, DGF and SGF can be divided into two parts, which correspond to consistent graph learning (Algorithm 2) and spectral clustering on the learned unified graph, respectively. We can see that our graph learning algorithm is very efficient and its running time is negligible when comparing to the running time of single-view spectral clustering, as shown in Table 3.

Moreover, all comparing multi-view algorithms in this paper require eigen-decomposition (ED) or singular value decomposition (SVD) of an n -by- n matrix at least two times (some require at least v times), while the proposed DGF

11. http://www.vision.caltech.edu/Image_Datasets/Caltech101/

12. <http://archive.ics.uci.edu/ml/datasets/Multiple+Features>

TABLE 2

Average clustering scores and standard deviation (%) over 10 runs by different multi-view spectral clustering methods; the best score and the second best score in each row are highlighted in bold and italic bold, respectively; the last two methods are our algorithms.

| Metric | Dataset | AASC | AWP | CoReg | MCGC | MVGL | RMSC | WMSC | SC (best) | SGF | DGF |
|--------|---------------|-----------------|------------------------|------------------------|-----------------|-----------------|------------------------|-----------------|------------------------|------------------------|------------------------|
| NMI | ORL | 86.74 \pm .87 | 85.60 \pm .00 | 90.49 \pm .71 | 89.39 \pm .00 | 83.79 \pm .00 | 90.67 \pm .62 | 90.33 \pm .52 | 90.78 \pm .50 | 91.14 \pm .31 | 91.80 \pm .17 |
| | Yale | 66.39 \pm 2.1 | 69.42 \pm .00 | 71.57 \pm .90 | 67.17 \pm .00 | 65.95 \pm .00 | 70.25 \pm 1.4 | 71.89 \pm .76 | 71.14 \pm .76 | 73.88 \pm .34 | 73.90 \pm .00 |
| | Reuters | 7.89 \pm .00 | 10.78 \pm .00 | 10.80 \pm .14 | 9.66 \pm .00 | 7.89 \pm .00 | 9.38 \pm .88 | 7.53 \pm .03 | 14.19 \pm .15 | 15.01 \pm .01 | 16.04 \pm .06 |
| | BBCSport | 64.20 \pm .00 | 78.13 \pm .00 | 91.87 \pm .00 | 79.62 \pm .00 | 68.05 \pm .00 | 71.77 \pm .00 | 67.72 \pm .00 | 87.11 \pm .00 | 93.96 \pm .00 | 92.68 \pm .00 |
| | NUS-WIDE | 17.83 \pm .43 | 15.96 \pm .00 | 18.95 \pm .12 | 14.55 \pm .00 | 5.50 \pm .00 | 18.95 \pm .29 | 19.03 \pm .22 | 17.33 \pm .33 | 19.69 \pm .12 | 19.86 \pm .26 |
| | Reuters-21578 | 11.06 \pm .00 | 10.54 \pm .00 | 29.80 \pm .25 | 11.43 \pm .00 | 8.63 \pm .00 | 13.28 \pm .31 | 25.81 \pm .88 | 27.27 \pm .13 | 31.49 \pm .09 | 30.94 \pm .06 |
| | MSRC-v1 | 69.78 \pm .14 | 67.71 \pm .00 | 74.57 \pm .09 | 71.80 \pm .00 | 65.58 \pm .00 | 68.87 \pm 1.9 | 72.11 \pm .40 | 64.78 \pm 1.0 | 78.88 \pm .07 | 80.98 \pm .00 |
| | CiteSeer | 15.74 \pm 1.6 | 8.90 \pm .00 | 34.16 \pm .02 | 17.99 \pm .00 | 1.48 \pm .00 | 33.39 \pm .00 | 32.22 \pm 2.1 | 17.63 \pm 1.1 | 37.16 \pm .11 | 38.10 \pm .07 |
| | ALOI | 35.68 \pm .50 | 69.90 \pm .00 | 85.36 \pm .57 | 69.75 \pm .01 | 46.94 \pm .00 | 82.45 \pm .68 | 84.22 \pm .17 | 80.18 \pm .45 | 90.90 \pm .35 | 91.08 \pm .33 |
| | Flower17 | 52.34 \pm 1.1 | 46.58 \pm .00 | 55.75 \pm 1.1 | 44.38 \pm .00 | 22.51 \pm .00 | 53.39 \pm .87 | 56.25 \pm .74 | 47.34 \pm .29 | 66.08 \pm .48 | 64.92 \pm .37 |
| | Caltech101 | 37.88 \pm .69 | 44.52 \pm .00 | 45.85 \pm .24 | 41.97 \pm .00 | 14.13 \pm .00 | 41.52 \pm .33 | 45.81 \pm .25 | 48.41 \pm .20 | 46.39 \pm .15 | 46.76 \pm .08 |
| | UCI Digits | 87.07 \pm .00 | 92.67 \pm .00 | 94.74 \pm .00 | 83.70 \pm .00 | 89.24 \pm .00 | 78.08 \pm 1.3 | 86.91 \pm .03 | 92.50 \pm .04 | 95.63 \pm .00 | 95.90 \pm .00 |
| ACC | ORL | 76.22 \pm 1.4 | 71.50 \pm .00 | 82.15 \pm 2.0 | 78.25 \pm .00 | 71.25 \pm .00 | 80.70 \pm 1.4 | 81.42 \pm 1.4 | 80.88 \pm .99 | 83.93 \pm .59 | 84.20 \pm .62 |
| | Yale | 65.88 \pm 1.5 | 67.27 \pm .00 | 68.42 \pm .34 | 61.82 \pm .00 | 64.85 \pm .00 | 68.79 \pm 1.4 | 69.70 \pm .57 | 69.21 \pm .75 | 70.79 \pm .26 | 70.91 \pm .00 |
| | Reuters | 19.75 \pm .00 | 25.17 \pm .00 | 24.41 \pm .26 | 23.92 \pm .00 | 19.67 \pm .00 | 23.50 \pm 1.7 | 21.00 \pm .00 | 29.38 \pm .26 | 29.95 \pm .07 | 31.64 \pm .06 |
| | BBCSport | 67.46 \pm .00 | 89.15 \pm .00 | 97.61 \pm .00 | 90.44 \pm .00 | 73.16 \pm .00 | 81.80 \pm .00 | 67.32 \pm .08 | 95.96 \pm .00 | 98.35 \pm .00 | 97.98 \pm .00 |
| | NUS-WIDE | 15.70 \pm .19 | 14.60 \pm .00 | 14.95 \pm .09 | 12.75 \pm .00 | 13.85 \pm .00 | 15.49 \pm .62 | 15.02 \pm .10 | 13.86 \pm .47 | 16.22 \pm .45 | 16.80 \pm .12 |
| | Reuters-21578 | 36.00 \pm .00 | 35.47 \pm .00 | 50.33 \pm .67 | 32.80 \pm .00 | 28.93 \pm .00 | 33.87 \pm .51 | 47.09 \pm .26 | 44.66 \pm .34 | 51.73 \pm .28 | 50.77 \pm .07 |
| | MSRC-v1 | 77.33 \pm .25 | 76.19 \pm .00 | 85.08 \pm .27 | 84.76 \pm .00 | 68.10 \pm .00 | 71.05 \pm 1.7 | 76.52 \pm .45 | 67.29 \pm .84 | 80.43 \pm .15 | 87.14 \pm .00 |
| | CiteSeer | 36.32 \pm 2.7 | 30.89 \pm .00 | 59.09 \pm .02 | 43.72 \pm .00 | 21.50 \pm .00 | 57.85 \pm .00 | 56.26 \pm 3.4 | 40.41 \pm 1.1 | 63.28 \pm .06 | 63.50 \pm .21 |
| | ALOI | 15.90 \pm .41 | 59.04 \pm .00 | 77.46 \pm 1.5 | 56.62 \pm .00 | 42.47 \pm .00 | 77.04 \pm 2.6 | 78.22 \pm .59 | 68.65 \pm 1.3 | 84.07 \pm 1.5 | 84.51 \pm 1.0 |
| | Flower17 | 51.62 \pm 1.4 | 44.85 \pm .00 | 55.96 \pm 2.0 | 43.90 \pm .00 | 25.00 \pm .00 | 54.00 \pm 2.1 | 55.88 \pm 1.4 | 43.47 \pm .97 | 69.15 \pm .90 | 67.03 \pm .97 |
| | Caltech101 | 23.80 \pm .77 | 26.22 \pm .00 | 25.34 \pm .93 | 23.00 \pm .00 | 13.44 \pm .00 | 22.77 \pm .93 | 23.29 \pm .67 | 26.74 \pm .54 | 24.04 \pm .45 | 23.53 \pm .39 |
| | UCI Digits | 84.55 \pm .00 | 96.85 \pm .00 | 97.65 \pm .00 | 82.40 \pm .00 | 86.05 \pm .00 | 78.94 \pm 2.0 | 87.02 \pm .04 | 96.59 \pm .03 | 98.10 \pm .00 | 98.25 \pm .00 |
| ARI | ORL | 62.89 \pm 2.4 | 66.34 \pm .00 | 75.38 \pm 1.8 | 70.76 \pm .00 | 46.00 \pm .00 | 75.19 \pm 1.6 | 74.44 \pm 1.4 | 74.63 \pm 1.3 | 76.76 \pm .81 | 78.24 \pm .40 |
| | Yale | 42.36 \pm 4.0 | 49.31 \pm .00 | 51.42 \pm 1.6 | 47.35 \pm .00 | 43.81 \pm .00 | 51.43 \pm 2.1 | 51.95 \pm 1.2 | 51.82 \pm 1.2 | 54.82 \pm .53 | 54.83 \pm .00 |
| | Reuters | 1.26 \pm .00 | 2.16 \pm .00 | 2.24 \pm .04 | 1.71 \pm .00 | 1.25 \pm .00 | 2.32 \pm .41 | 1.64 \pm .00 | 6.00 \pm .07 | 6.53 \pm .02 | 8.34 \pm .06 |
| | BBCSport | 52.33 \pm .00 | 80.45 \pm .00 | 93.92 \pm .00 | 79.83 \pm .00 | 58.35 \pm .00 | 70.78 \pm .00 | 55.43 \pm .02 | 89.75 \pm .00 | 95.53 \pm .00 | 94.76 \pm .00 |
| | NUS-WIDE | 4.13 \pm .18 | 3.75 \pm .00 | 4.85 \pm .11 | 2.43 \pm .00 | 0.16 \pm .00 | 4.53 \pm .30 | 4.71 \pm .12 | 4.38 \pm .23 | 4.97 \pm .21 | 5.96 \pm .20 |
| | Reuters-21578 | 2.44 \pm .00 | 3.02 \pm .00 | 19.25 \pm .27 | 2.87 \pm .00 | 0.24 \pm .00 | 3.22 \pm .50 | 17.23 \pm .30 | 23.09 \pm .44 | 23.49 \pm .08 | 21.50 \pm .04 |
| | MSRC-v1 | 59.90 \pm .18 | 62.25 \pm .00 | 69.47 \pm .66 | 68.09 \pm .00 | 49.67 \pm .00 | 55.03 \pm 2.4 | 65.02 \pm .55 | 54.40 \pm 1.4 | 72.28 \pm .10 | 75.35 \pm .00 |
| | CiteSeer | 12.08 \pm 1.2 | 2.99 \pm .00 | 31.92 \pm .02 | 12.11 \pm .00 | -0.02 \pm .00 | 24.97 \pm .00 | 25.45 \pm .53 | 10.12 \pm .54 | 37.44 \pm .05 | 37.94 \pm .18 |
| | ALOI | 6.39 \pm .34 | 47.42 \pm .00 | 69.15 \pm 1.6 | 41.61 \pm .01 | 2.48 \pm .00 | 65.61 \pm 1.5 | 68.03 \pm .52 | 56.13 \pm 1.8 | 78.32 \pm 1.2 | 78.84 \pm 1.2 |
| | Flower17 | 28.82 \pm 2.2 | 30.36 \pm .00 | 39.13 \pm 2.0 | 27.51 \pm .00 | 3.02 \pm .00 | 36.77 \pm 1.6 | 40.24 \pm 1.1 | 26.89 \pm .60 | 52.61 \pm .74 | 50.83 \pm .75 |
| | Caltech101 | 7.18 \pm 1.5 | 15.28 \pm .00 | 17.33 \pm 1.1 | 13.84 \pm .00 | -0.55 \pm .00 | 21.57 \pm 1.7 | 15.39 \pm .92 | 16.45 \pm .53 | 14.71 \pm .65 | 14.28 \pm .47 |
| | UCI Digits | 81.26 \pm .00 | 93.14 \pm .00 | 94.86 \pm .00 | 76.81 \pm .00 | 83.78 \pm .00 | 71.37 \pm 2.2 | 82.22 \pm .04 | 92.60 \pm .06 | 95.82 \pm .00 | 96.15 \pm .00 |
| purity | ORL | 80.20 \pm 1.2 | 72.75 \pm .00 | 84.82 \pm 1.2 | 83.00 \pm .00 | 77.00 \pm .00 | 84.60 \pm 1.1 | 84.40 \pm 1.1 | 83.80 \pm .93 | 86.40 \pm .44 | 87.03 \pm .49 |
| | Yale | 66.00 \pm 1.5 | 67.88 \pm .00 | 68.48 \pm .29 | 63.03 \pm .00 | 64.85 \pm .00 | 69.27 \pm 1.3 | 69.70 \pm .57 | 70.24 \pm .78 | 70.79 \pm .26 | 70.91 \pm .00 |
| | Reuters | 24.00 \pm .00 | 28.33 \pm .00 | 28.09 \pm .21 | 28.08 \pm .00 | 24.00 \pm .00 | 27.23 \pm 1.6 | 25.08 \pm .00 | 34.09 \pm .05 | 34.42 \pm .00 | 35.23 \pm .05 |
| | BBCSport | 74.26 \pm .00 | 89.15 \pm .00 | 97.61 \pm .00 | 90.44 \pm .00 | 75.55 \pm .00 | 82.17 \pm .00 | 74.82 \pm .00 | 95.96 \pm .00 | 98.35 \pm .00 | 97.98 \pm .00 |
| | NUS-WIDE | 23.92 \pm .40 | 22.85 \pm .00 | 24.92 \pm .14 | 22.40 \pm .00 | 15.70 \pm .00 | 24.48 \pm .30 | 25.68 \pm .53 | 25.75 \pm .34 | 25.86 \pm .43 | 26.77 \pm .31 |
| | Reuters-21578 | 38.07 \pm .00 | 37.67 \pm .00 | 56.97 \pm .25 | 43.47 \pm .00 | 33.00 \pm .00 | 44.05 \pm .36 | 51.95 \pm 1.4 | 52.11 \pm .05 | 58.07 \pm .28 | 57.15 \pm .04 |
| | MSRC-v1 | 77.33 \pm .25 | 79.52 \pm .00 | 85.08 \pm .27 | 84.76 \pm .00 | 72.86 \pm .00 | 76.14 \pm 1.8 | 81.14 \pm .25 | 73.19 \pm .81 | 83.81 \pm .00 | 87.14 \pm .00 |
| | CiteSeer | 36.99 \pm 2.7 | 31.31 \pm .00 | 62.30 \pm .02 | 46.32 \pm .00 | 22.22 \pm .00 | 59.87 \pm .00 | 58.00 \pm 3.2 | 41.51 \pm .98 | 65.78 \pm .05 | 66.35 \pm .06 |
| | ALOI | 18.40 \pm .36 | 60.25 \pm .00 | 78.49 \pm 1.2 | 60.39 \pm .00 | 44.98 \pm .00 | 78.44 \pm 2.3 | 79.78 \pm .47 | 70.41 \pm 1.1 | 86.08 \pm 1.1 | 86.41 \pm .79 |
| | Flower17 | 54.56 \pm 1.2 | 47.87 \pm .00 | 59.85 \pm 1.4 | 47.72 \pm .00 | 26.47 \pm .00 | 56.36 \pm 1.3 | 59.73 \pm 1.2 | 47.96 \pm .60 | 71.10 \pm .80 | 68.90 \pm .98 |
| | Caltech101 | 40.11 \pm .39 | 42.79 \pm .00 | 45.83 \pm .44 | 43.12 \pm .00 | 21.46 \pm .00 | 38.98 \pm .34 | 45.94 \pm .37 | 48.34 \pm .18 | 46.26 \pm .21 | 46.28 \pm .34 |
| | UCI Digits | 87.00 \pm .00 | 96.85 \pm .00 | 97.65 \pm .00 | 84.75 \pm .00 | 88.10 \pm .00 | 81.41 \pm 1.4 | 87.02 \pm .04 | 96.59 \pm .03 | 98.10 \pm .00 | 98.25 \pm .00 |

and SGF perform ED only once (when running spectral clustering on the unified graph). Since ED and SVD have at least $\Omega(n^2)$ time complexity [39], which is the complexity bottleneck in many multi-view clustering algorithms, our multi-view clustering algorithms are likely to run several times faster than the comparing multi-view algorithms on

very large datasets.

6.7 Consistency, Inconsistency and Robustness Issues

In Figure 1, we see that the learned unified graph by SGF is “cleaner” than any single view and clearly contains

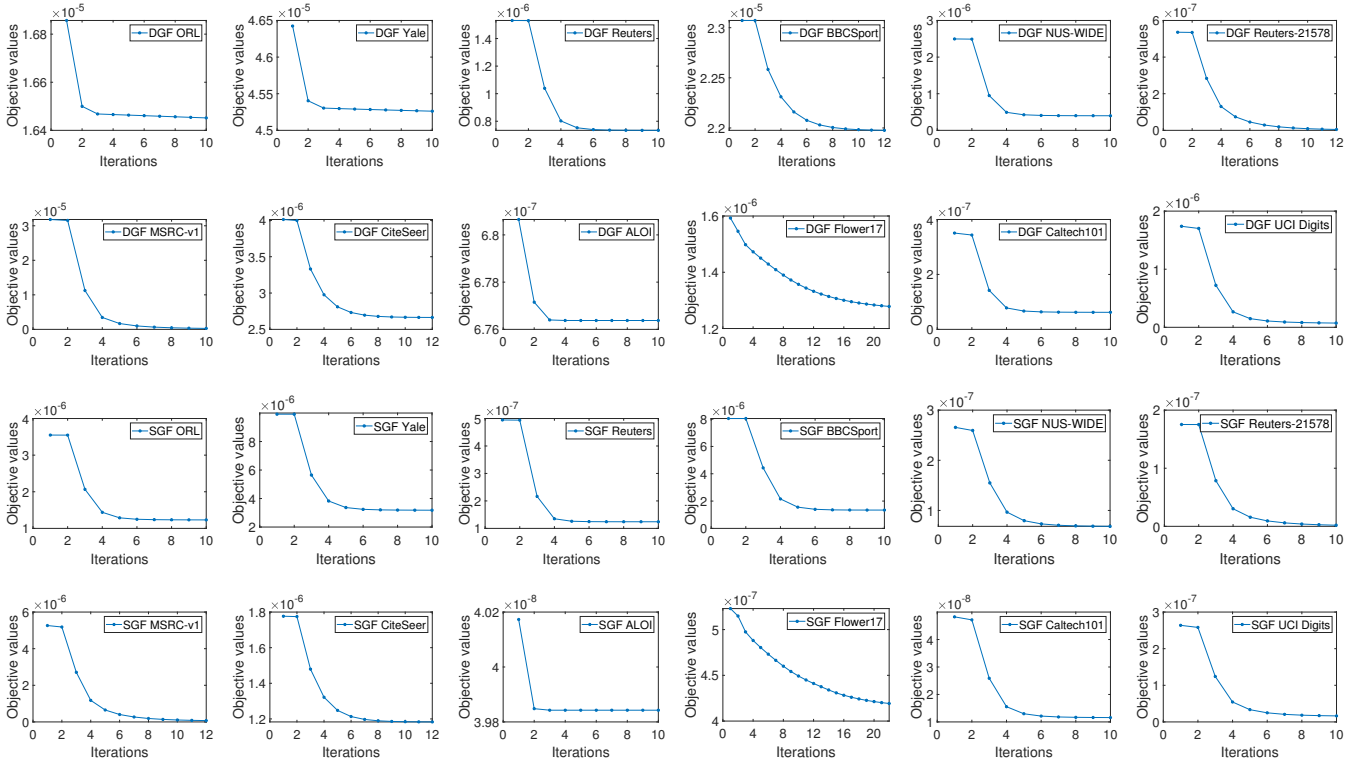


Fig. 2. Convergence curves of the proposed algorithms DGF and SGF on the 12 datasets. The first two rows correspond to DGF, and the last two rows correspond to SGF (please note that the datasets ordering is the same as that in Table 2, in case the dataset labels are illegible). Note: the objective values are very small because we have normalized all adjacency matrices before performing consistent graph learning to improve convergence (see Section 4.3).

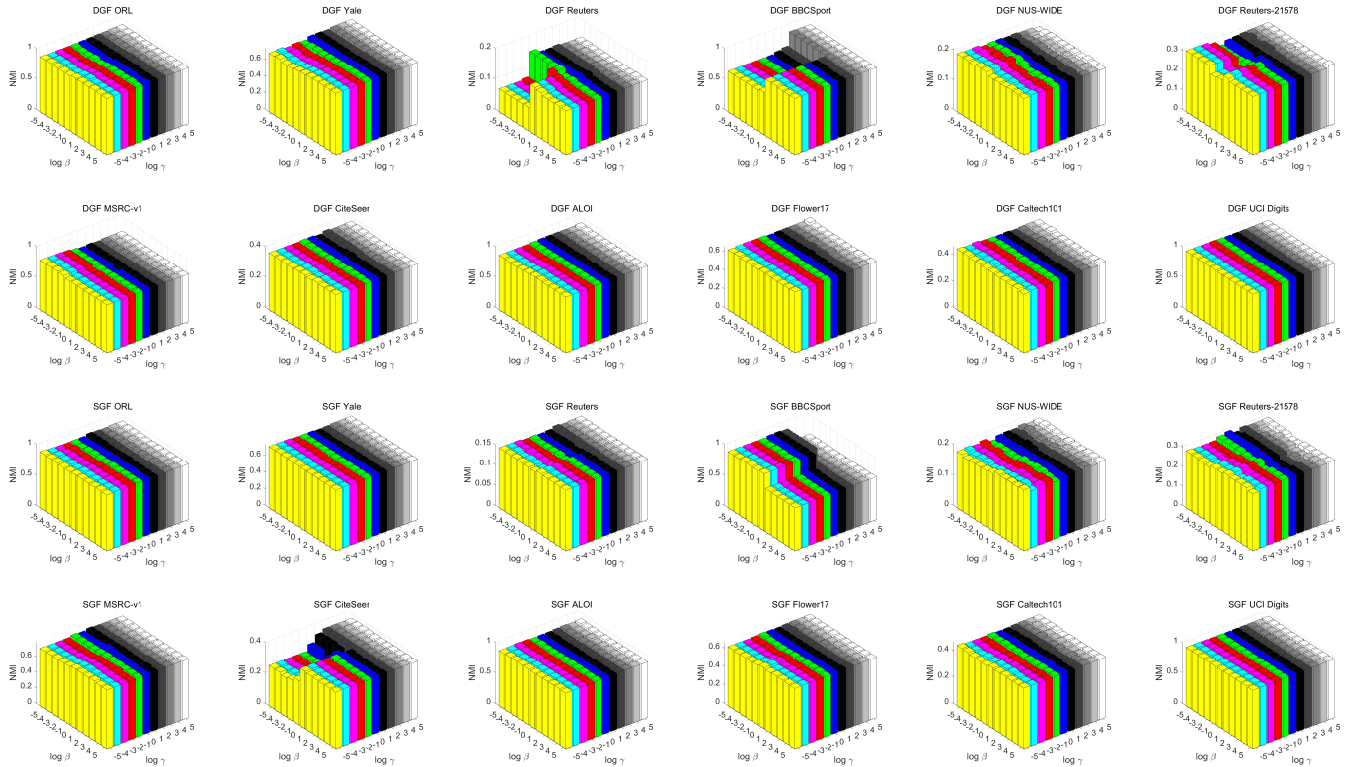


Fig. 3. NMI against parameters β and γ of DGF and SGF on the 12 datasets. The first two rows correspond to DGF, and the last two rows correspond to SGF (please note that the datasets ordering is the same as that in Table 2, in case the dataset labels are illegible).

TABLE 3

Average running time and standard deviation (in seconds) over 10 runs by different methods, where the time is recorded from constructing distance graphs to obtaining clustering result (i.e., the entire process); DGF-GL and SGF-GL stand for the running time of Consistent Graph Learning (Algorithm 2) in DGF and SGF, respectively; the running time of the fastest two multi-view clustering methods in each row (without counting single-view SC) is highlighted in bold.

| Dataset | AASC | AWP | CoReg | MCGC | MVGL | RMSC | WMSC | SC (best) | DGF | SGF | DGF-GL | SGF-GL |
|---------------|----------------|-----------------------|----------------|-----------------|----------------|----------------|-----------------------|----------------|-----------------------|-----------------------|-----------------|-----------------|
| ORL | 0.36 \pm .00 | 0.26 \pm .00 | 7.11 \pm .19 | 1.05 \pm .02 | 3.97 \pm .02 | 3.00 \pm .02 | 0.32 \pm .00 | 0.26 \pm .00 | 0.36 \pm .00 | 0.37 \pm .00 | .003 \pm .000 | .003 \pm .000 |
| Yale | 0.14 \pm .00 | 0.07 \pm .00 | 0.41 \pm .03 | 0.87 \pm .01 | 1.00 \pm .02 | 0.11 \pm .00 | 0.09 \pm .00 | 0.07 \pm .00 | 0.10 \pm .00 | 0.11 \pm .00 | .002 \pm .000 | .002 \pm .000 |
| Reuters | 0.66 \pm .00 | 0.62 \pm .01 | 1.97 \pm .04 | 7.77 \pm .02 | 36.8 \pm .02 | 12.9 \pm .02 | 0.66 \pm .00 | 0.50 \pm .00 | 0.67 \pm .00 | 0.65 \pm .00 | 0.01 \pm .00 | 0.01 \pm .00 |
| BBCSport | 0.13 \pm .01 | 0.10 \pm .00 | 3.75 \pm .02 | 0.95 \pm .02 | 7.62 \pm .02 | 0.50 \pm .01 | 0.12 \pm .00 | 0.10 \pm .00 | 0.13 \pm .00 | 0.12 \pm .00 | .007 \pm .001 | .004 \pm .000 |
| NUS-WIDE | 2.47 \pm .03 | 0.90 \pm .02 | 14.8 \pm .06 | 55.8 \pm .11 | 54.3 \pm .05 | 36.8 \pm .11 | 1.24 \pm .02 | 0.60 \pm .01 | 1.17 \pm .01 | 1.17 \pm .00 | 0.03 \pm .00 | 0.05 \pm .00 |
| Reuters-21578 | 1.70 \pm .01 | 1.64 \pm .02 | 5.75 \pm .05 | 10.00 \pm .02 | 61.8 \pm .04 | 5.31 \pm .02 | 1.69 \pm .01 | 1.46 \pm .00 | 1.68 \pm .00 | 1.68 \pm .00 | 0.02 \pm .00 | 0.01 \pm .00 |
| MSRC-v1 | 0.22 \pm .01 | 0.04 \pm .00 | 2.17 \pm .02 | 0.40 \pm .01 | 1.36 \pm .02 | 0.37 \pm .01 | 0.06 \pm .00 | 0.04 \pm .00 | 0.06 \pm .00 | 0.06 \pm .00 | .003 \pm .000 | .003 \pm .000 |
| CiteSeer | 1.44 \pm .01 | 1.18 \pm .01 | 118 \pm .09 | 36.6 \pm .02 | 203 \pm .07 | 419 \pm 1.6 | 1.32 \pm .01 | 1.01 \pm .01 | 1.38 \pm .02 | 1.40 \pm .02 | 0.02 \pm .00 | 0.02 \pm .00 |
| ALOI | 39.4 \pm .41 | 36.1 \pm .18 | 2545 \pm 7.0 | 713 \pm .21 | 5330 \pm 6.1 | 388 \pm 1.4 | 71.7 \pm .08 | 18.7 \pm .06 | 14.4 \pm .04 | 14.3 \pm .03 | 0.16 \pm .00 | 0.11 \pm .00 |
| Flower17 | 0.70 \pm .01 | 0.38 \pm .01 | 50.0 \pm .19 | 24.3 \pm .04 | 69.3 \pm .04 | 9.21 \pm .21 | 0.49 \pm .00 | 0.10 \pm .01 | 0.37 \pm .01 | 0.38 \pm .00 | 0.03 \pm .00 | 0.03 \pm .00 |
| Caltech101 | 42.5 \pm .14 | 38.8 \pm .03 | 294 \pm .60 | 1129 \pm .49 | 7274 \pm 8.5 | 2062 \pm 8.0 | 41.2 \pm .07 | 30.2 \pm .07 | 39.2 \pm .02 | 39.3 \pm .01 | 0.17 \pm .00 | 0.17 \pm .00 |
| UCI Digits | 1.02 \pm .01 | 1.33 \pm .03 | 352 \pm .68 | 15.7 \pm .03 | 79.5 \pm .05 | 22.5 \pm 1.6 | 3.06 \pm .01 | 0.60 \pm .01 | 0.92 \pm .01 | 0.93 \pm .01 | 0.03 \pm .00 | 0.03 \pm .00 |

the consistent parts of all views. By the motivation of the consistent graph learning framework in Section 3, *it always learns a better graph if the consistent part of multi-view graphs is the dominant part*, which also means that the inconsistent parts are sparse across views. In other words, we do not claim that the proposed framework can learn a better graph in all circumstances, which is unlikely to happen because no learning algorithms are universal [40]. But it can learn a better graph under the reasonable assumption that the information provided by different views is complementary and not severely conflicting. In experiment, we do see in Caltech101 the best single-view SC is slightly better than our algorithms as well as other multi-view clustering methods, which might be caused by the severely conflicting views of Caltech101. Under such circumstances, multi-view clustering methods are unlikely to perform well.

7 CONCLUSIONS

This paper presents a novel multi-view graph learning approach, which for the first time simultaneously and explicitly models multi-view consistency as well as multi-view inconsistency in a unified optimization model, where multi-view consistency can be iteratively learned and fused into a unified graph as the multi-view inconsistency is automatically identified and removed. To solve this model, we theoretically analyze the properties of the optimization problem, based on which we design an efficient algorithm that has basically linear time complexity in the number of edges on the multi-view graphs, even though exactly solving the problem is NP-hard. The proposed framework is further extended to two graph fusion versions, which correspond to distance (dissimilarity) graph fusion and similarity graph fusion, respectively. Our framework can accept user-defined weights to consider the importance of each view and has good performance even without parameter tuning. Experimental results demonstrate the superiority, efficiency and robustness of the proposed algorithms against several state-of-the-art multi-view spectral clustering algorithms on the 12 real-world datasets.

ACKNOWLEDGMENTS

This work was supported by NSFC(61976097 and 61876193).

APPENDIX A

MORE DETAIL ABOUT THE DATASETS

The 12 real-world datasets are described by various multi-view features, as shown in Table 4, where the meaning of multi-view features is listed as follows: CENTRIST descriptor (CENT) [41], Color Histogram (CH), Color Moments (CM), color correlation (CORR), Color Similarity (CS), Edge Direction Histogram (EDH), profile correlations (FAC), Fourier coefficients of character shapes (FOU), Gabor feature (Gabor), GIST descriptor (GIST) [42], Haralick features (HAR) [43], Histogram of Oriented Gradients (HOG) [44], HSB color histograms (HSB), HSV color features (HSV), Karhunen-Love coefficients (KAR) Local Binary Patterns (LBP), morphological features (MOR), RGB color histograms (RGB), SIFT internal/boundary features (SIFT int/bdy) [45], Wavelet Texture (WT), Zernike moment (ZER) [46].

APPENDIX B

PERFORMANCE OF THE PROPOSED FRAMEWORK WITHOUT PARAMETER TUNING

In the parameter analysis of the proposed algorithms, we have shown that DGF and SGF have stable performance across a wide range of parameters. In the section, we show that, even without dataset-specific parameter tuning, DGF and SGF can still achieve comparable or better performance against the state-of-the-art multi-view clustering algorithms in the real-world datasets. In accordance with the proposed graph learning framework, we fix the two hyperparameters by simply setting $\beta = 1$ and $\gamma = 10^4$, which is a reasonable combination since β controls the magnitude of the inconsistent parts of all views and γ would penalize the objective value if the consistent parts were incorrectly moved to the inconsistent parts. The performance of DGF and SGF with fixed hyperparameters is shown in Table 5. For comparison, the scores of other algorithms *with parameter tuning* are copied from Table 2 in the main text to Table 5. We can see that in most datasets, DGF and SGF *without parameter tuning* obtain better scores than other algorithms *with parameter tuning* (if any), while in other datasets DGF and SGF without parameter tuning generally perform comparably well with the best algorithms.

TABLE 4
Statistics and multi-view features (# dimensions) of the real-world datasets.

| Dataset | # views | # classes | # instances | View 1 | View 2 | View 3 | View 4 | View 5 | View 6 | View 7 |
|-----------------------|---------|-----------|-------------|-----------------|---------------|---------------|----------------|----------------|----------|----------|
| ORL | 3 | 40 | 400 | Intensity(4096) | LBP(3304) | Gabor(6750) | | | | |
| Yale | 3 | 15 | 165 | Intensity(4096) | LBP(3304) | Gabor(6750) | | | | |
| Reuters | 5 | 6 | 1200 | English(2000) | French(2000) | German(2000) | Italian(2000) | Spanish(2000) | | |
| BBCSport | 2 | 5 | 544 | seg1(3183) | seg2(3203) | | | | | |
| NUS-WIDE | 5 | 31 | 2000 | CH(65) | CM(226) | CORR(145) | EDH(74) | WT(129) | | |
| Reuters-21578 | 5 | 6 | 1500 | English(21531) | France(24892) | German(34251) | Italian(15506) | Spanish(11547) | | |
| MSRC-v1 | 5 | 7 | 210 | CM(24) | HOG(576) | GIST(512) | LBP(256) | CENT(254) | | |
| CiteSeer | 2 | 6 | 3312 | citations(3312) | content(3703) | | | | | |
| ALOI | 4 | 100 | 10800 | CS(77) | HAR(13) | HSB(64) | RGB(125) | | | |
| Flower17 ^a | 7 | 17 | 1360 | Color | Texture | Shape | HOG | HSV | SIFT bdy | SIFT int |
| Caltech101 | 6 | 102 | 9144 | Gabor(48) | WM(40) | CENT(254) | HOG(1984) | GIST(512) | LBP(928) | |
| UCI Digits | 6 | 10 | 2000 | PIX(240) | FOU(76) | FAC(216) | ZER(47) | KAR(64) | MOR(6) | |

^aOnly distance matrices are available.

REFERENCES

- [1] A. K. Jain, "Data clustering: 50 years beyond k -means," *Pattern Recognition Letters*, vol. 31, no. 8, pp. 651–666, 2010.
- [2] J. Shi and J. Malik, "Normalized cuts and image segmentation," *IEEE Transactions on Pattern Analysis and Machine Intelligence*, vol. 22, no. 8, pp. 888–905, 2000.
- [3] A. Y. Ng, M. I. Jordan, and Y. Weiss, "On spectral clustering: Analysis and an algorithm," in *Advances in neural information processing systems*, 2002, pp. 849–856.
- [4] U. Von Luxburg, "A tutorial on spectral clustering," *Statistics and computing*, vol. 17, no. 4, pp. 395–416, 2007.
- [5] F. Nie, X. Wang, and H. Huang, "Clustering and projected clustering with adaptive neighbors," in *Proceedings of the 20th ACM SIGKDD International Conference on Knowledge Discovery and Data Mining*, 2014, pp. 977–986.
- [6] F. Nie, X. Wang, M. I. Jordan, and H. Huang, "The constrained laplacian rank algorithm for graph-based clustering," in *Thirtieth AAAI Conference on Artificial Intelligence*, 2016.
- [7] K. Zhan, C. Zhang, J. Guan, and J. Wang, "Graph learning for multiview clustering," *IEEE Transactions on Cybernetics*, vol. 48, no. 10, pp. 2887–2895, 2018.
- [8] K. Zhan, C. Niu, C. Chen, F. Nie, C. Zhang, and Y. Yang, "Graph structure fusion for multiview clustering," *IEEE Transactions on Knowledge and Data Engineering*, 2018.
- [9] K. Zhan, F. Nie, J. Wang, and Y. Yang, "Multiview consensus graph clustering," *IEEE Transactions on Image Processing*, vol. 28, no. 3, pp. 1261–1270, March 2019.
- [10] F. Nie, J. Li, and X. Li, "Self-weighted multiview clustering with multiple graphs," in *IJCAI*, 2017, pp. 2564–2570.
- [11] A. Bojchevski, Y. Matkovic, and S. Günnemann, "Robust spectral clustering for noisy data: Modeling sparse corruptions improves latent embeddings," in *Proceedings of the 23rd ACM SIGKDD International Conference on Knowledge Discovery and Data Mining*. ACM, 2017, pp. 737–746.
- [12] Y. Liang, D. Huang, and C.-D. Wang, "Consistency meets inconsistency: A unified graph learning framework for multi-view clustering," in *Proceedings of the IEEE International Conference on Data Mining*, 2019.
- [13] L. T. H. An and P. D. Tao, "A branch and bound method via d.c. optimization algorithms and ellipsoidal technique for box constrained nonconvex quadratic problems," *Journal of Global Optimization*, vol. 13, no. 2, pp. 171–206, 1998.
- [14] S. Bickel and T. Scheffer, "Multi-view clustering," in *ICDM*, vol. 4, 2004, pp. 19–26.
- [15] A. Blum and T. Mitchell, "Combining labeled and unlabeled data with co-training," in *Proceedings of the eleventh annual conference on Computational learning theory*. ACM, 1998, pp. 92–100.
- [16] A. Kumar, P. Rai, and H. Daumé, "Co-regularized multi-view spectral clustering," in *Advances in Neural Information Processing Systems*, 2011, pp. 1413–1421.
- [17] Y. Wang, W. Zhang, L. Wu, X. Lin, M. Fang, and S. Pan, "Iterative views agreement: An iterative low-rank based structured optimization method to multi-view spectral clustering," *arXiv preprint arXiv:1608.05560*, 2016.
- [18] L. Zong, X. Zhang, X. Liu, and H. Yu, "Weighted multi-view spectral clustering based on spectral perturbation," in *Thirty-Second AAAI Conference on Artificial Intelligence*, 2018.
- [19] Y. Wang, L. Wu, X. Lin, and J. Gao, "Multiview spectral clustering via structured low-rank matrix factorization," *IEEE transactions on neural networks and learning systems*, no. 99, pp. 1–11, 2018.
- [20] R. Xia, Y. Pan, L. Du, and J. Yin, "Robust multi-view spectral clustering via low-rank and sparse decomposition," in *Twenty-Eighth AAAI Conference on Artificial Intelligence*, 2014.
- [21] F. Nie, L. Tian, and X. Li, "Multiview clustering via adaptively weighted procrustes," in *Proceedings of the 24th ACM SIGKDD International Conference on Knowledge Discovery & Data Mining*. ACM, 2018, pp. 2022–2030.
- [22] H.-C. Huang, Y.-Y. Chuang, and C.-S. Chen, "Affinity aggregation for spectral clustering," in *2012 IEEE Conference on Computer Vision and Pattern Recognition*. IEEE, 2012, pp. 773–780.
- [23] R.-C. Li and L.-H. Zhang, "Convergence of the block lanczos method for eigenvalue clusters," *Numerische Mathematik*, vol. 131, no. 1, pp. 83–113, 2015.
- [24] S. Burer and A. N. Letchford, "On nonconvex quadratic programming with box constraints," *SIAM Journal on Optimization*, vol. 20, no. 2, pp. 1073–1089, 2009.
- [25] Y. Liang, "Gradient projection for solving quadratic programs with standard simplex constraints," *arXiv preprint arXiv:2006.06934*, 2020.
- [26] W. W. Hager and H. Zhang, "A new active set algorithm for box constrained optimization," *SIAM Journal on Optimization*, vol. 17, no. 2, pp. 526–557, 2006.
- [27] A. Cristofari, M. De Santis, S. Lucidi, and F. Rinaldi, "An active-set algorithmic framework for non-convex optimization problems over the simplex," *Computational Optimization and Applications*, pp. 1–33, 2018.
- [28] M. L. Eaton and M. D. Perlman, "The non-singularity of generalized sample covariance matrices," *The Annals of Statistics*, pp. 710–717, 1973.
- [29] D. C. Sorensen, "Implicitly restarted arnoldi/lanczos methods for large scale eigenvalue calculations," in *Parallel Numerical Algorithms*. Springer, 1997, pp. 119–165.
- [30] T. Y. Hou, D. Huang, K. C. Lam, and Z. Zhang, "A fast hierarchically preconditioned eigensolver based on multiresolution matrix decomposition," *Multiscale Modeling & Simulation*, vol. 17, no. 1, pp. 260–306, 2019.
- [31] T.-S. Chua, J. Tang, R. Hong, H. Li, Z. Luo, and Y.-T. Zheng, "Nus-wide: A real-world web image database from national university of singapore," in *Proc. of ACM Conf. on Image and Video Retrieval (CIVR'09)*, Santorini, Greece, July 8–10, 2009.
- [32] J. Winn and N. Jojic, "Locus: Learning object classes with unsupervised segmentation," in *Tenth IEEE International Conference on Computer Vision (ICCV'05) Volume 1*, vol. 1. IEEE, 2005, pp. 756–763.

TABLE 5

Average clustering scores and standard deviation (%) over 10 runs by different multi-view spectral clustering methods, where the parameters of our methods (SGF and DGF) are fixed (with $\beta = 1$, $\gamma = 10^4$); the best score and the second best score in each row are highlighted in bold and italic bold, respectively; the last two methods are our algorithms.

| Metric | Dataset | AASC | AWP | CoReg | MCGC | MVGL | RMSC | WMSC | SC (best) | SGF | DGF |
|--------|---------------|-----------------|------------------------|------------------------|------------------------|-----------------|------------------------|-----------------|------------------------|------------------------|------------------------|
| NMI | ORL | 86.74 \pm .87 | 85.60 \pm .00 | 90.49 \pm .71 | 89.39 \pm .00 | 83.79 \pm .00 | 90.67 \pm .62 | 90.33 \pm .52 | 90.78 \pm .50 | 91.02 \pm .43 | 91.59 \pm .41 |
| | Yale | 66.39 \pm 2.1 | 69.42 \pm .00 | 71.57 \pm .90 | 67.17 \pm .00 | 65.95 \pm .00 | 70.25 \pm 1.4 | 71.89 \pm .76 | 71.14 \pm .76 | 73.25 \pm .16 | 73.90 \pm .00 |
| | Reuters | 7.89 \pm .00 | 10.78 \pm .00 | 10.80 \pm .14 | 9.66 \pm .00 | 7.89 \pm .00 | 9.38 \pm .88 | 7.53 \pm .03 | 14.19 \pm .15 | 14.86 \pm .06 | 14.47 \pm .00 |
| | BBCSport | 64.20 \pm .00 | 78.13 \pm .00 | 91.87 \pm .00 | 79.62 \pm .00 | 68.05 \pm .00 | 71.77 \pm .00 | 67.72 \pm .00 | 87.11 \pm .00 | 69.82 \pm .00 | 92.11 \pm .00 |
| | NUS-WIDE | 17.83 \pm .43 | 15.96 \pm .00 | 18.95 \pm .12 | 14.55 \pm .00 | 5.50 \pm .00 | 18.95 \pm .29 | 19.03 \pm .22 | 17.33 \pm .33 | 19.51 \pm .38 | 19.18 \pm .12 |
| | Reuters-21578 | 11.06 \pm .00 | 10.54 \pm .00 | 29.80 \pm .25 | 11.43 \pm .00 | 8.63 \pm .00 | 13.28 \pm .31 | 25.81 \pm .88 | 27.27 \pm .13 | 30.44 \pm .00 | 30.56 \pm .00 |
| | MSRC-v1 | 69.78 \pm .14 | 67.71 \pm .00 | 74.57 \pm .09 | 71.80 \pm .00 | 65.58 \pm .00 | 68.87 \pm 1.9 | 72.11 \pm .40 | 64.78 \pm 1.0 | 76.52 \pm .36 | 77.69 \pm .06 |
| | CiteSeer | 15.74 \pm 1.6 | 8.90 \pm .00 | 34.16 \pm .02 | 17.99 \pm .00 | 1.48 \pm .00 | 33.39 \pm .00 | 32.22 \pm 2.1 | 17.63 \pm 1.1 | 37.07 \pm .03 | 37.19 \pm .18 |
| | ALOI | 35.68 \pm .50 | 69.90 \pm .00 | 85.36 \pm .57 | 69.75 \pm .01 | 46.94 \pm .00 | 82.45 \pm .68 | 84.22 \pm .17 | 80.18 \pm .45 | 90.72 \pm .27 | 90.72 \pm .48 |
| | Flower17 | 52.34 \pm 1.1 | 46.58 \pm .00 | 55.75 \pm 1.1 | 44.38 \pm .00 | 22.51 \pm .00 | 53.39 \pm .87 | 56.25 \pm .74 | 47.34 \pm .29 | 65.50 \pm .16 | 64.65 \pm .43 |
| | Caltech101 | 37.88 \pm .69 | 44.52 \pm .00 | 45.85 \pm .24 | 41.97 \pm .00 | 14.13 \pm .00 | 41.52 \pm .33 | 45.81 \pm .25 | 48.41 \pm .20 | 46.28 \pm .09 | 45.35 \pm .17 |
| | UCI Digits | 87.07 \pm .00 | 92.67 \pm .00 | 94.74 \pm .00 | 83.70 \pm .00 | 89.24 \pm .00 | 78.08 \pm 1.3 | 86.91 \pm .03 | 92.50 \pm .04 | 95.42 \pm .00 | 95.15 \pm .00 |
| ACC | ORL | 76.22 \pm 1.4 | 71.50 \pm .00 | 82.15 \pm 2.0 | 78.25 \pm .00 | 71.25 \pm .00 | 80.70 \pm 1.4 | 81.42 \pm 1.4 | 80.88 \pm .99 | 83.85 \pm 1.1 | 84.25 \pm 1.2 |
| | Yale | 65.88 \pm 1.5 | 67.27 \pm .00 | 68.42 \pm .34 | 61.82 \pm .00 | 64.85 \pm .00 | 68.79 \pm 1.4 | 69.70 \pm .57 | 69.21 \pm .75 | 70.91 \pm .00 | 70.91 \pm .00 |
| | Reuters | 19.75 \pm .00 | 25.17 \pm .00 | 24.41 \pm .26 | 23.92 \pm .00 | 19.67 \pm .00 | 23.50 \pm 1.7 | 21.00 \pm .00 | 29.38 \pm .26 | 29.88 \pm .04 | 29.75 \pm .00 |
| | BBCSport | 67.46 \pm .00 | 89.15 \pm .00 | 97.61 \pm .00 | 90.44 \pm .00 | 73.16 \pm .00 | 81.80 \pm .00 | 67.32 \pm .08 | 95.96 \pm .00 | 71.88 \pm .00 | 97.79 \pm .00 |
| | NUS-WIDE | 15.70 \pm .19 | 14.60 \pm .00 | 14.95 \pm .09 | 12.75 \pm .00 | 13.85 \pm .00 | 15.49 \pm .62 | 15.02 \pm .10 | 13.86 \pm .47 | 16.55 \pm .31 | 15.96 \pm .38 |
| | Reuters-21578 | 36.00 \pm .00 | 35.47 \pm .00 | 50.33 \pm .67 | 32.80 \pm .00 | 28.93 \pm .00 | 33.87 \pm .51 | 47.09 \pm .26 | 44.66 \pm .34 | 51.40 \pm .00 | 51.07 \pm .00 |
| | MSRC-v1 | 77.33 \pm .25 | 76.19 \pm .00 | 85.08 \pm .27 | 84.76 \pm .00 | 68.10 \pm .00 | 71.05 \pm 1.7 | 76.52 \pm .45 | 67.29 \pm .84 | 81.81 \pm .44 | 79.10 \pm .15 |
| | CiteSeer | 36.32 \pm 2.7 | 30.89 \pm .00 | 59.09 \pm .02 | 43.72 \pm .00 | 21.50 \pm .00 | 57.85 \pm .00 | 56.26 \pm 3.4 | 40.41 \pm 1.1 | 63.19 \pm .07 | 63.89 \pm .24 |
| | ALOI | 15.90 \pm .41 | 59.04 \pm .00 | 77.46 \pm 1.5 | 56.62 \pm .00 | 42.47 \pm .00 | 77.04 \pm 2.6 | 78.22 \pm .59 | 68.65 \pm 1.3 | 83.62 \pm 1.2 | 83.33 \pm 1.8 |
| | Flower17 | 51.62 \pm 1.4 | 44.85 \pm .00 | 55.96 \pm 2.0 | 43.90 \pm .00 | 25.00 \pm .00 | 54.00 \pm 2.1 | 55.88 \pm 1.4 | 43.47 \pm .97 | 66.80 \pm .68 | 66.85 \pm .91 |
| | Caltech101 | 23.80 \pm .77 | 26.22 \pm .00 | 25.34 \pm .93 | 23.00 \pm .00 | 13.44 \pm .00 | 22.77 \pm .93 | 23.29 \pm .67 | 26.74 \pm .54 | 23.93 \pm .39 | 23.05 \pm .32 |
| | UCI Digits | 84.55 \pm .00 | 96.85 \pm .00 | 97.65 \pm .00 | 82.40 \pm .00 | 86.05 \pm .00 | 78.94 \pm 2.0 | 87.02 \pm .04 | 96.59 \pm .03 | 98.00 \pm .00 | 97.90 \pm .00 |
| ARI | ORL | 62.89 \pm 2.4 | 66.34 \pm .00 | 75.38 \pm 1.8 | 70.76 \pm .00 | 46.00 \pm .00 | 75.19 \pm 1.6 | 74.44 \pm 1.4 | 74.63 \pm 1.3 | 76.56 \pm 1.1 | 77.79 \pm .93 |
| | Yale | 42.36 \pm 4.0 | 49.31 \pm .00 | 51.42 \pm 1.6 | 47.35 \pm .00 | 43.81 \pm .00 | 51.43 \pm 2.1 | 51.95 \pm 1.2 | 51.82 \pm 1.2 | 54.58 \pm .14 | 54.83 \pm .00 |
| | Reuters | 1.26 \pm .00 | 2.16 \pm .00 | 2.24 \pm .04 | 1.71 \pm .00 | 1.25 \pm .00 | 2.32 \pm .41 | 1.64 \pm .00 | 6.00 \pm .07 | 6.46 \pm .01 | 6.34 \pm .00 |
| | BBCSport | 52.33 \pm .00 | 80.45 \pm .00 | 93.92 \pm .00 | 79.83 \pm .00 | 58.35 \pm .00 | 70.78 \pm .00 | 55.43 \pm .02 | 89.75 \pm .00 | 60.49 \pm .00 | 94.30 \pm .00 |
| | NUS-WIDE | 4.13 \pm .18 | 3.75 \pm .00 | 4.85 \pm .11 | 2.43 \pm .00 | 0.16 \pm .00 | 4.53 \pm .30 | 4.71 \pm .12 | 4.38 \pm .23 | 5.19 \pm .12 | 5.02 \pm .22 |
| | Reuters-21578 | 2.44 \pm .00 | 3.02 \pm .00 | 19.25 \pm .27 | 2.87 \pm .00 | 0.24 \pm .00 | 3.22 \pm .50 | 17.23 \pm .30 | 23.09 \pm .44 | 23.91 \pm .00 | 23.54 \pm .00 |
| | MSRC-v1 | 59.90 \pm .18 | 62.25 \pm .00 | 69.47 \pm .66 | 68.09 \pm .00 | 49.67 \pm .00 | 55.03 \pm 2.4 | 65.02 \pm .55 | 54.40 \pm 1.4 | 70.28 \pm .27 | 70.61 \pm .08 |
| | CiteSeer | 12.08 \pm 1.2 | 2.99 \pm .00 | 31.92 \pm .02 | 12.11 \pm .00 | -0.02 \pm .00 | 24.97 \pm .00 | 25.45 \pm .53 | 10.12 \pm .54 | 37.35 \pm .06 | 37.68 \pm .31 |
| | ALOI | 6.39 \pm .34 | 47.42 \pm .00 | 69.15 \pm 1.6 | 41.61 \pm .01 | 2.48 \pm .00 | 65.61 \pm 1.5 | 68.03 \pm .52 | 56.13 \pm 1.8 | 77.86 \pm 1.0 | 77.63 \pm 1.7 |
| | Flower17 | 28.82 \pm 2.2 | 30.36 \pm .00 | 39.13 \pm 2.0 | 27.51 \pm .00 | 3.02 \pm .00 | 36.77 \pm 1.6 | 40.24 \pm 1.1 | 26.89 \pm .60 | 51.10 \pm .33 | 50.49 \pm .69 |
| | Caltech101 | 7.18 \pm 1.5 | 15.28 \pm .00 | 17.33 \pm 1.1 | 13.84 \pm .00 | -0.55 \pm .00 | 21.57 \pm 1.7 | 15.39 \pm .92 | 16.45 \pm .53 | 14.76 \pm .58 | 14.52 \pm .47 |
| | UCI Digits | 81.26 \pm .00 | 93.14 \pm .00 | 94.86 \pm .00 | 76.81 \pm .00 | 83.78 \pm .00 | 71.37 \pm 2.2 | 82.22 \pm .04 | 92.60 \pm .06 | 95.60 \pm .00 | 95.38 \pm .00 |
| purity | ORL | 80.20 \pm 1.2 | 72.75 \pm .00 | 84.82 \pm 1.2 | 83.00 \pm .00 | 77.00 \pm .00 | 84.60 \pm 1.1 | 84.40 \pm 1.1 | 83.80 \pm .93 | 86.28 \pm .65 | 86.73 \pm .55 |
| | Yale | 66.00 \pm 1.5 | 67.88 \pm .00 | 68.48 \pm .29 | 63.03 \pm .00 | 64.85 \pm .00 | 69.27 \pm 1.3 | 69.70 \pm .57 | 70.24 \pm .78 | 70.91 \pm .00 | 70.91 \pm .00 |
| | Reuters | 24.00 \pm .00 | 28.33 \pm .00 | 28.09 \pm .21 | 28.08 \pm .00 | 24.00 \pm .00 | 27.23 \pm 1.6 | 25.08 \pm .00 | 34.09 \pm .05 | 34.33 \pm .00 | 34.33 \pm .00 |
| | BBCSport | 74.26 \pm .00 | 89.15 \pm .00 | 97.61 \pm .00 | 90.44 \pm .00 | 75.55 \pm .00 | 82.17 \pm .00 | 74.82 \pm .00 | 95.96 \pm .00 | 75.74 \pm .00 | 97.79 \pm .00 |
| | NUS-WIDE | 23.92 \pm .40 | 22.85 \pm .00 | 24.92 \pm .14 | 22.40 \pm .00 | 15.70 \pm .00 | 24.48 \pm .30 | 25.68 \pm .53 | 25.75 \pm .34 | 25.87 \pm .34 | 25.97 \pm .24 |
| | Reuters-21578 | 38.07 \pm .00 | 37.67 \pm .00 | 56.97 \pm .25 | 43.47 \pm .00 | 33.00 \pm .00 | 44.05 \pm .36 | 51.95 \pm 1.4 | 52.11 \pm .05 | 57.73 \pm .00 | 57.33 \pm .00 |
| | MSRC-v1 | 77.33 \pm .25 | 79.52 \pm .00 | 85.08 \pm .27 | 84.76 \pm .00 | 72.86 \pm .00 | 76.14 \pm 1.8 | 81.14 \pm .25 | 73.19 \pm .81 | 83.14 \pm .25 | 83.33 \pm .00 |
| | CiteSeer | 36.99 \pm 2.7 | 31.31 \pm .00 | 62.30 \pm .02 | 46.32 \pm .00 | 22.22 \pm .00 | 59.87 \pm .00 | 58.00 \pm 3.2 | 41.51 \pm .98 | 65.73 \pm .03 | 66.24 \pm .17 |
| | ALOI | 18.40 \pm .36 | 60.25 \pm .00 | 78.49 \pm 1.2 | 60.39 \pm .00 | 44.98 \pm .00 | 78.44 \pm 2.3 | 79.78 \pm .47 | 70.41 \pm 1.1 | 85.60 \pm .93 | 85.58 \pm 1.3 |
| | Flower17 | 54.56 \pm 1.2 | 47.87 \pm .00 | 59.85 \pm 1.4 | 47.72 \pm .00 | 26.47 \pm .00 | 56.36 \pm 1.3 | 59.73 \pm 1.2 | 47.96 \pm .60 | 69.09 \pm .53 | 68.92 \pm .85 |
| | Caltech101 | 40.11 \pm .39 | 42.79 \pm .00 | 45.83 \pm .44 | 43.12 \pm .00 | 21.46 \pm .00 | 38.98 \pm .34 | 45.94 \pm .37 | 48.34 \pm .18 | 45.98 \pm .30 | 45.03 \pm .37 |
| | UCI Digits | 87.00 \pm .00 | 96.85 \pm .00 | 97.65 \pm .00 | 84.75 \pm .00 | 88.10 \pm .00 | 81.41 \pm 1.4 | 87.02 \pm .04 | 96.59 \pm .03 | 98.00 \pm .00 | 97.90 \pm .00 |

- [33] J.-M. Geusebroek, G. J. Burghouts, and A. W.-M. Smeulders, "The amsterdam library of object images," *International Journal of Computer Vision*, vol. 61, no. 1, pp. 103–112, 2005.
- [34] M. E. Houle, V. Oria, S. Satoh, and J. Sun, "Knowledge propagation in large image databases using neighborhood information," in *Proceedings of the 19th ACM international conference on Multimedia*, 2011, pp. 1033–1036.
- [35] M.-E. Nilsback and A. Zisserman, "A visual vocabulary for flower classification," in *2006 IEEE Computer Society Conference on Computer Vision and Pattern Recognition (CVPR'06)*, vol. 2. IEEE, 2006, pp. 1447–1454.
- [36] —, "Automated flower classification over a large number of classes," in *2008 Sixth Indian Conference on Computer Vision, Graphics & Image Processing*. IEEE, 2008, pp. 722–729.
- [37] A. Strehl and J. Ghosh, "Cluster ensembles—a knowledge reuse framework for combining multiple partitions," *Journal of machine learning research*, vol. 3, no. Dec, pp. 583–617, 2002.
- [38] N. X. Vinh, J. Epps, and J. Bailey, "Information theoretic measures for clusterings comparison: Variants, properties, normalization and correction for chance," *Journal of Machine Learning Research*, vol. 11, no. Oct, pp. 2837–2854, 2010.
- [39] Y. Saad, *Numerical methods for large eigenvalue problems: revised edition*. SIAM, 2011.
- [40] S. Shalev-Shwartz and S. Ben-David, *Understanding machine learning: From theory to algorithms*. Cambridge university press, 2014.
- [41] J. Wu and J. M. Rehg, "Centrist: A visual descriptor for scene categorization," *IEEE Transactions on Pattern Analysis and Machine Intelligence*, vol. 33, no. 8, pp. 1489–1501, 2010.
- [42] A. Oliva and A. Torralba, "Modeling the shape of the scene: A holistic representation of the spatial envelope," *International journal of computer vision*, vol. 42, no. 3, pp. 145–175, 2001.
- [43] R. M. Haralick, K. Shanmugam, and I. H. Dinstein, "Textural features for image classification," *IEEE Transactions on systems, man, and cybernetics*, no. 6, pp. 610–621, 1973.
- [44] N. Dalal and B. Triggs, "Histograms of oriented gradients for human detection," in *2005 IEEE computer society conference on computer vision and pattern recognition (CVPR'05)*, vol. 1. IEEE, 2005, pp. 886–893.
- [45] D. G. Lowe, "Distinctive image features from scale-invariant keypoints," *International journal of computer vision*, vol. 60, no. 2, pp. 91–110, 2004.
- [46] C.-H. Teh and R. T. Chin, "On image analysis by the methods of moments," *IEEE Transactions on pattern analysis and machine intelligence*, vol. 10, no. 4, pp. 496–513, 1988.